GEOLOGIC MAP OF THE MONTANA PART OF THE SALMON 30' X 60' QUADRANGLE, SOUTHWESTERN MONTANA

Pamphlet to Accompany Map

Mapped by:

Jeffrey D. Lonn,[1] Colleen G. Elliott,[1] Reed S. Lewis,[2] Russell F. Burmester,[2] Mark D. McFaddan,[2] Loudon R. Stanford,[2] and Susanne U. Jänecke[3]

[1]Montana Bureau of Mines and Geology

[2]Idaho Geological Survey

[3]Utah State University

Partial support provided by the STATEMAP component of the National Cooperative Geologic Mapping Program of the U.S. Geological Survey under Contract G13AC00210

MBMG
Montana Bureau of Mines and Geology

Cover image: View south along the Continental Divide in the northern Beaverhead Mountains showing west-dipping, overturned quartzite of the Swauger Formation. Photo by Jeffrey D. Lonn, MBMG.

GEOLOGIC MAP OF THE MONTANA PART OF THE SALMON 30' x 60' QUADRANGLE, SOUTHWESTERN MONTANA

Pamphlet to Accompany Map

Montana Bureau of Mines and Geology Geologic Map 75

Mapped by:

Jeffrey D. Lonn,[1] Colleen G. Elliott,[1] Reed S. Lewis,[2] Russell F. Burmester,[2] Mark D. McFaddan,[2] Loudon R. Stanford,[2] and Susanne U. Jänecke[3]

[1]Montana Bureau of Mines and Geology

[2]Idaho Geological Survey

[3]Utah State University

CONTENTS

FIGURES

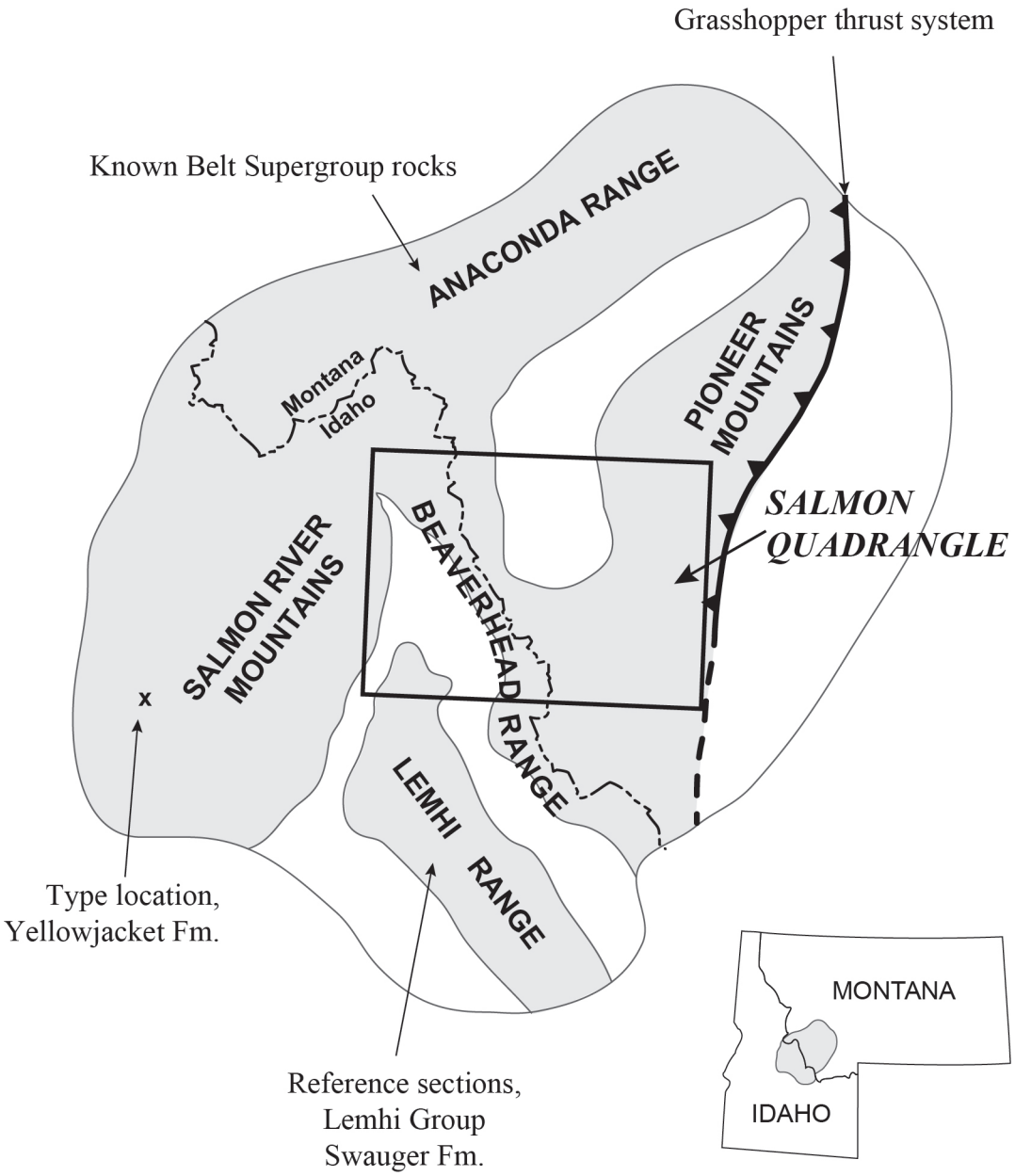

Figure 1. Location of Salmon 30′ x 60′ quadrangle with respect to known Belt Supergroup rocks and the reference and type sections of the Lemhi Group and Yellowjacket Formation. Shaded areas represent mountain ranges containing Mesoproterozoic sedimentary rocks.

INTRODUCTION

One of the challenges to geologists in the northern Rocky Mountains is understanding the relationships between the Mesoproterozoic Belt Supergroup and the age-equivalent Lemhi strata of east-central Idaho (fig. 1). To address this problem, a collaborative Montana Bureau of Mines and Geology (MBMG)–Idaho Geological Survey (IGS) 1:24,000-scale mapping project began in 2007 along the Montana–Idaho border within the Salmon 30' x 60' quadrangle. The collaborative team mapped 16 7.5' quadrangles before compiling this 1:100,000-scale bedrock map that clarifies major structures and regional stratigraphic relationships. The Idaho part of the Salmon 30′ x 60′ quadrangle was previously released by the IGS (Burmester and others, 2016a).

GEOLOGIC SUMMARY

The Salmon 30′ x 60′ quadrangle is largely underlain by Mesoproterozoic strata and unconsolidated Tertiary deposits. The immensely thick (>15 km) succession of Mesoproterozoic siliciclastic sediments (fig. 2 and Description of Map Units) represents strata that were deposited in the Lemhi subbasin, a southern arm of the larger Belt Basin (Burmester and others, 2013, 2016a,b). These Lemhi subbasin strata, which are sandier than typical Belt Supergroup units, extend north and northeast into Montana where they grade into the Missoula Group of the upper Belt Supergroup (fig. 2; Lonn, 2014; Lonn and others, 2016a,b). The eastern margin of the Lemhi subbasin, composed of Archean and Paleoproterozoic crystalline rocks, is located immediately to the east of the Salmon quad-

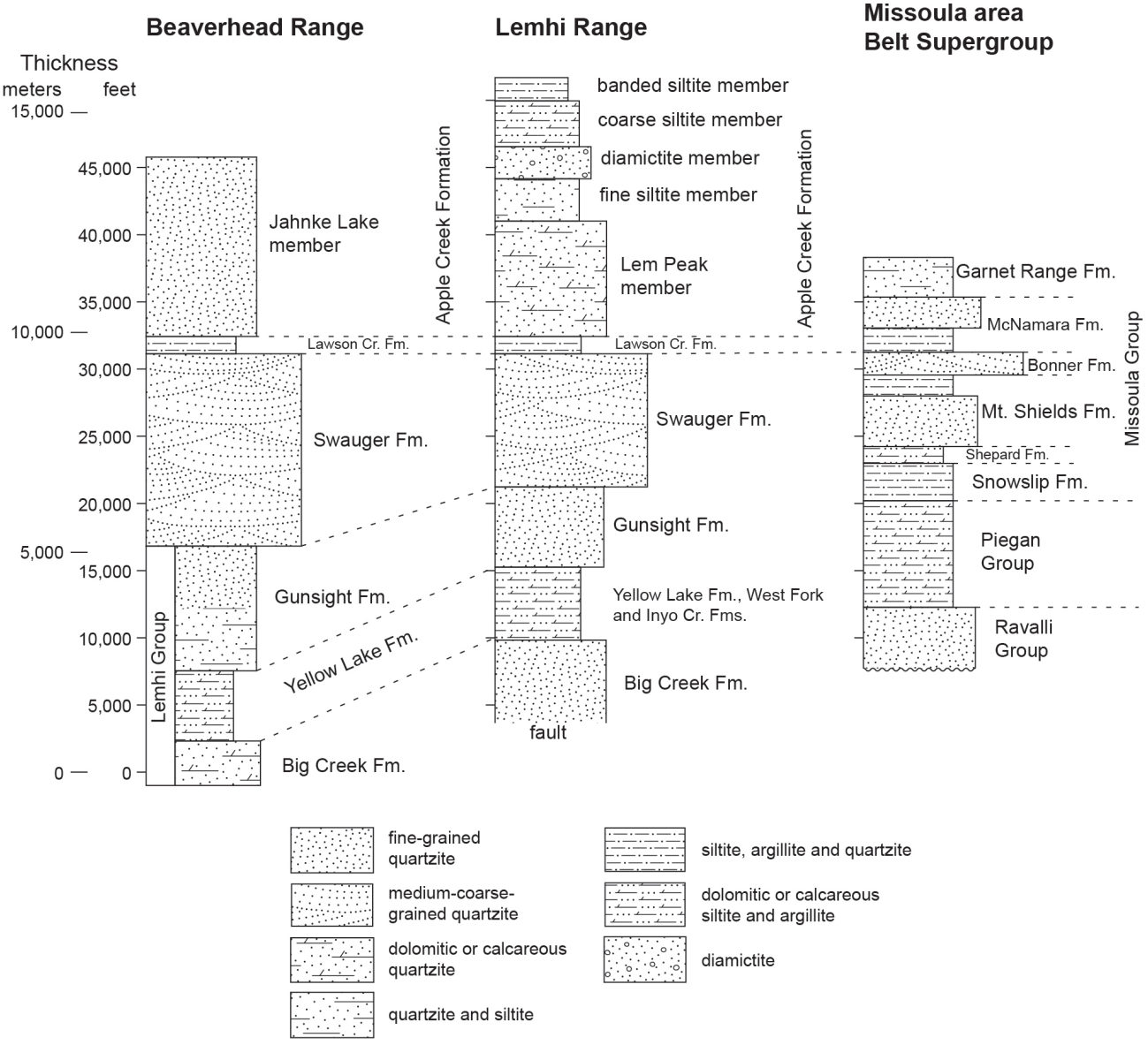

Figure 2. Correlations between Mesoproterozoic strata of the Salmon quadrangle (Beaverhead Range), type sections of Lemhi subbasin strata (Lemhi Range), and upper Belt Supergroup strata near Missoula, Montana. From Lonn and others, 2016b.

rangle (McDonald and Lonn, 2013). Following deposition, these sediments experienced multiple tectonic events. The complex geologic history is summarized below:

1. Intrusion of 1,370 Ma granites occurred shortly after deposition of the Mesoproterozoic sediments ceased. The granite is exposed in the Salmon River Mountains on the Idaho part of the Salmon quadrangle (Burmester and others, 2016a) west of this map.
2. Garnets dated at 1.1 Ga (Jeff Vervoort, written commun., 2013) in some strata of the Beaverhead Mountains indicate metamorphism and tectonism. Explanation of the garnets and their significance awaits further mapping and petrography.
3. Phanerozoic strata presumably were deposited disconformably over the Mesoproterozoic rocks, although they are preserved only in the easternmost part of the map.
4. Cretaceous northeast–southwest shortening deformed the thick sedimentary pile into huge northwest-trending, northeast-verging folds, probably during early stages of the Sevier Orogeny (Tysdal, 2002; Lonn and others, 2013b; 2016c). An enormous, overturned, east-facing fold limb is spectacularly exposed in the Beaverhead Mountains east of the Freeman Thrust along the western boundary of the map (see cross-section A–A′ on plate 1, and fig. 3). Figure 3 illustrates the magnitude of the fold whose amplitude is greater than 10 km. Although folds of this scale seem unreasonable, east- to northeast-verging folds of similar size occur in the thick Mesoproterozoic strata of the Lemhi Range in Idaho (Tysdal, 2002) and in northwestern Montana (Harrison and Cressman, 1993). These enormous folds are culminations in the fold-and-thrust belt and influenced sediment-dispersal patterns for tens of millions of years during and after their creation (Jänecke and others, 2000).
5. Subsequent east–west shortening dissected the earliest folds along a system of northwest-striking reverse and normal faults with strike-slip components (Lonn and others, 2013c; 2016b). The resulting major faults of the quadrangle (fault map on plate 1)—the North Fork Thrust, Freeman Thrust, Eastern Strand of the Beaverhead Divide Fault, and the Jackson–Buffalo Creek Fault Zone—formed during this, probably Late Cretaceous, time, along with the Grasshopper Thrust system exposed just east of the quadrangle (Ruppel and others, 1993).
6. Between about 81 Ma and 46 Ma intrusive activity was widespread in the northeast and northwest parts of the quadrangle. The younger activity is inferred to be related to extensional tectonism and Challis volcanism.
7. Significant Tertiary extension affected the entire region, producing the many normal faults that bound the Tertiary valleys such as the Meriwether Lewis Fault and Muddy–Grasshopper Detachment, and reactivating preexisting fabrics and faults, including both strands of the Beaverhead Divide Fault, the Moose Creek Fault, and the Jackson–Buffalo Creek Fault Zone (plate 1). Two main periods of extension occurred: late Eocene to early Miocene extension was dominated by detachment faults, whereas cross-cutting Basin and Range extension is Miocene to Quaternary (VanDenburg and others, 1998; Jänecke, 2007). The Muddy–Grasshopper Detachment on the southeast edge of the Salmon quadrangle had top-west movement during Eocene and early Oligocene time, forming the basin in which the Medicine Lodge beds were syntectonically deposited (Jänecke and others, 1999, 2001, 2005). The detachment flattens at about 1.5 km depth and had 5–10 km of slip (Kickham, 2002; Matoush, 2002; Jänecke and others, 2005).
8. Oligocene basalt flows (27–28 Ma; Jänecke and others, 2005) at the top of the Medicine Lodge beds were folded and faulted prior to deposition of the Everson Creek beds in Oligocene to early Miocene time. Jänecke (1994), Stroup and others (2008), Roe (2010), and Barber (2013) report detrital zircon data and paleocurrent indicators in the Everson Creek beds that suggest the Big Hole and Grasshopper basins were once linked. They document paleoflow towards the south and southeast across the divide between the upper Big Hole and Grasshopper Valleys.

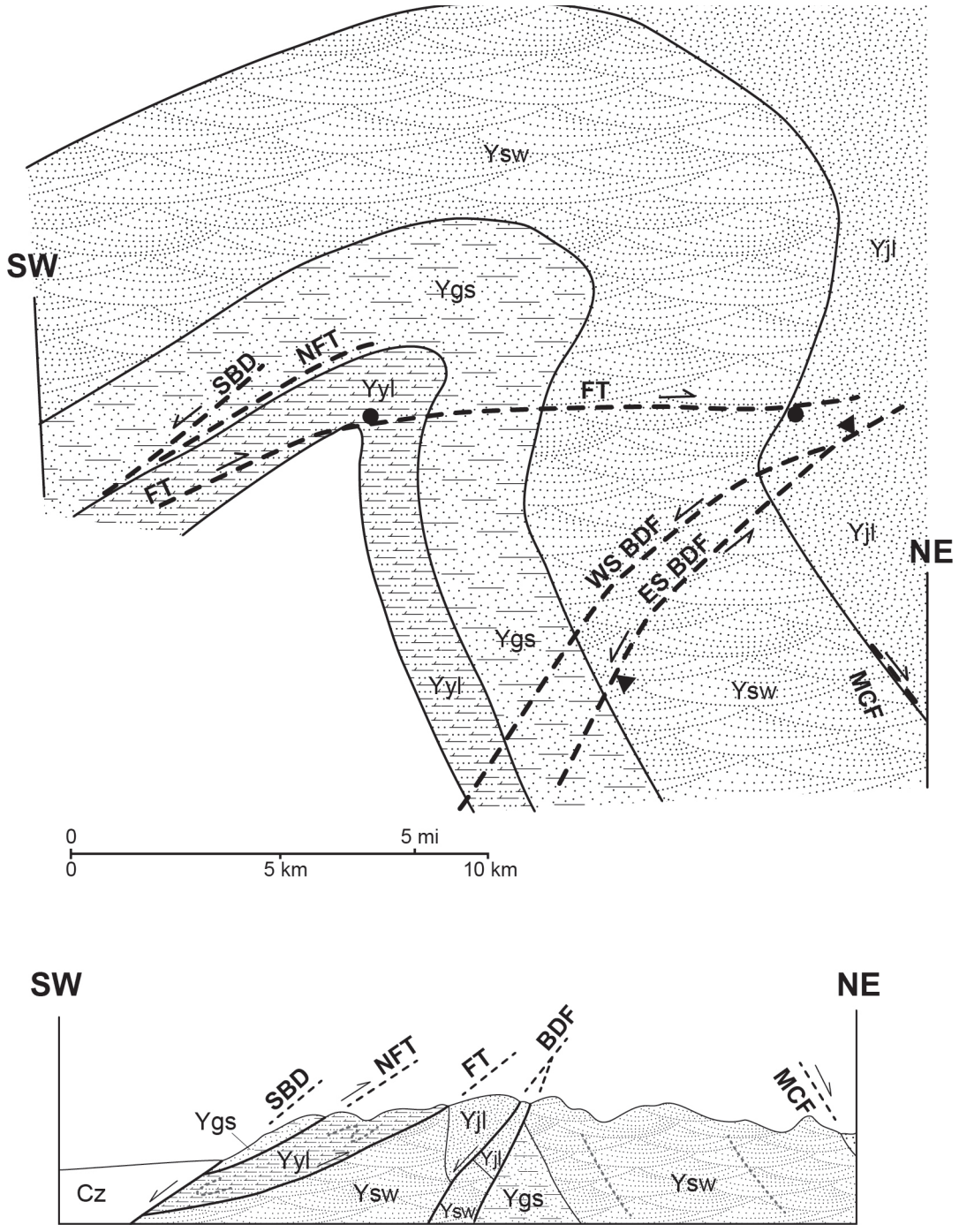

Figure 3. Sketch of a cross section drawn across the Beaverhead Range, northwest of cross section A–A', restored to pre-fault geometry by realigning stratigraphic contacts. Black circles along FT and black triangles along ES BDF show modern erosion levels restored to pre-fault locations and represent net offset along faults. SBD, Salmon basin detachment; FT, Freeman Thrust; NFT, North Fork Thrust; WS BDF, western strand Beaverhead Divide Fault; ES BDF, eastern strand Beaverhead Divide Fault; MCF, Moose Creek Fault; Cz, undivided Cenozoic sediments; other units as on plate 1. After Lonn and others, 2016b.

9. The total amount of Tertiary and younger extension within the Salmon quadrangle is unknown, but it must have been considerable. Drillhole and geophysical data within the Big Hole Valley north of the quadrangle show that the valley is as deep as 4,850 m (15,900 ft; Roe, 2010). The region is still extending as part of the Basin and Range province, and fault scarps cutting Quaternary deposits were observed in several places (Jänecke and others, 1999; Kickham, 2002; Matoush, 2002; Jänecke and others, 2005; Jänecke, 2007; Lonn and others, 2006; Lonn and Lewis, 2012; Lewis and others, 2009a).

10. Pediments developed in the Grasshopper basin across faulted and folded basin-fill (Jänecke and others, 2005). These were partially mantled with gravel and colluvium. Numerous landslide deposits formed, mostly in the Tertiary sediments.
11. In the Pleistocene, the high elevations of the Beaverhead and Pioneer Mountains were extensively glaciated several times. Much of the bedrock along the eastern flank of the Beaverhead Mountains is covered by till and outwash.

Descriptions of Major Faults (plate 1)

Interpretations of the major faults are largely summarized from Lonn and others (2016b).

North Fork and Freeman Thrusts

The North Fork and Freeman Thrusts along the western border of the map strike northwest, dip gently southwest, and are closely parallel up to where they merge in the southwestern part of the map. Each has a parallel left-stepping bend near cross section A–A′. Mylonitic lineations plunge due west, and shear sense indicators show top-to-the-east, sinistral-reverse movement. Because the fault plane strikes north–northwest, and lineations plunge due west, a component of left-lateral offset must be included. Both faults appear to have formed simultaneously as an east-directed thrust system. However, the correlation of the hanging wall units in both faults is uncertain (see Description of Map Units section for more detail), and therefore, amount of offset is unknown. Figure 3 interprets the Freeman Thrust as an older-over-younger fault, with offset estimated to be more than 10 km (Lonn and others, 2016b). An alternative is that the Freeman Thrust is a younger-over-older thrust with amount of offset then being unknown. The hanging wall unit of the structurally higher North Fork Thrust is also of uncertain affinity, but both alternatives interpret the North Fork Thrust as a younger-over-older thrust.

Western Strand of the Beaverhead Divide Fault

The Western Strand of the Beaverhead Divide Fault (WS BDF) strikes northwest, dips 35–65° southwest (cross section A-A′), and exhibits normal-sense stratigraphic offset. Thin sections show mylonitic foliation defined by ribbons of recrystallized quartz separated by phyllosilicate films, with poorly developed lineations and shear sense indicators. The fault is locally intruded by 46 Ma (Richard Gaschnig, written commun., 2009) mafic dikes that are commonly mylonitic with well developed, due-west-plunging lineations. S-C fabrics show west-side-down, oblique-normal movement, confirming the normal-sense stratigraphic offset. Some movement along this fault occurred after 46 Ma, although earlier activity may have also occurred.

Eastern Strand of the Beaverhead Divide Fault

The Eastern Strand Beaverhead Divide Fault (ES BDF) is a generally northwest-striking, steeply southwest-dipping fault that closely parallels the structurally higher Freeman Thrust, even along the left-stepping bend. Lonn and others (2016b) interpret the fault parallelism, the proximity of mylonitic foliation and sheath folds, and the occurrence of a horse of Paleoproterozoic crystalline basement on its southeastern segment to suggest initial compression, even though stratigraphic offset is normal-sense along its entire length. There are no obvious shear sense indicators to help solve this paradox.

Both hanging wall and footwall of the ES BDF contain parallel, very thick, east-facing homoclines of Lemhi strata (plate 1), and the simplest explanation for this similarity is that both sides were originally part of the same giant fold limb (Lonn and others, 2016b). Figure 3 shows how the observed geometry might have formed by dissection of single giant, northeast-verging anticline along the North Fork Thrust, Freeman Thrust, WS BDF, and dextral-normal-sense ES BDF. Normal-sense offset on the ES BDF is interpreted to have occurred in a compressive environment at approximately the same time as the Freeman–North Fork thrust systems were active. Perhaps the ES BDF footwall was initially a southwest-directed, northeast-dipping reverse fault that has been rotated into its present southwest-dipping orientation. Or perhaps the northeast side was extruded or popped up between the ES BDF and a fault further east such as the Moose Creek Fault discussed below. In the southwestern part of the map, a horse of Paleoproterozoic crystalline basement occurs along the ES BDF between a down-to-the-southwest normal fault and the down-to-the-northeast Monument Fault, which also supports the hypothesis that the ES BDF developed initially as a contractional fault.

Tertiary, down-to-the-west, normal movement on the ES BDF is indicated by Tertiary deposits preserved along both its southernmost and northernmost segments (Lonn and others, 2013a; Lewis and others, 2009a) and by breccia along its fault plane south of the Carmen Creek stock (Lonn and others, 2008). Although all movement on the ES BDF could be attributed to Tertiary extension, it seems more probable that northwest-striking segments of the Cretaceous fault were reactivated in a Tertiary extensional setting. Offset on the ES BDF is approximately 4–8 km (2.5–5 mi; Lonn and others, 2016b).

The southern, extensional, end of the ES BDF was named the Bloody Dick Fault by Coppinger (1974), a name that continues to be used (e.g., Sherwin and others, 2017).

Moose Creek Fault

A northwest-striking, steeply northeast-dipping fault system with normal-sense stratigraphic offset extends along the eastern flank of the Beaverhead Range in the northern part of the map. East-dipping cleavage and outcrop-scale drag folds near the fault suggest down-to-the-northeast normal-sense movement. Although stratigraphic displacement is small across the Moose Creek Fault, it might be a component of the Tertiary fault system responsible for the great depth of the Big Hole Basin.

Buffalo Creek–Jackson Fault

The poorly exposed Buffalo Creek–Jackson Fault strikes north to northwest and separates dissimilar Mesoproterozoic sections. No Apple Creek Formation is preserved on the northeast side; in its place, the Lawson Creek Formation is very thick and coarse grained. The Buffalo Creek Fault could represent either a Cretaceous thrust with significant displacement or a reactivated Mesoproterozoic growth fault.

Monument Fault

The Monument Fault juxtaposes Paleoproterozoic gneiss against Mesoproterozoic quartzite on the southern edge of the quadrangle. There are at least five possible interpretations for the fault:

1. Reverse fault dipping south, placing older rocks over younger (Coppinger, 1974; Sherwin and others, 2017),
2. Steeply dipping southwest-side-up fault that is part of the complex Beaverhead Divide fault system (Lonn and others, 2016b),
3. Vertical left-lateral Great Divide Megashear that juxtaposes the Belt and Lemhi basins (O'Neill and others, 2007),
4. North–northeast-dipping reverse fault that places younger rocks over older rocks (Ruppel and others, 1993),
5. No fault at all, but an angular unconformity folded into an upright anticline (S. Jänecke and C. Elliott, unpublished).

A 2017 conference field trip to the fault had the goal of reaching a consensus (Elliott and Lonn, 2017). It was agreed that Belt rocks structurally overlie basement at the southeast end of the fault, and that the northwest end of the fault has the characteristics of a vertical shear zone. Otherwise, there was no consensus.

Grasshopper Thrust (also known as the Kelley Thrust)

Just beyond the eastern edge of the map, the north-striking, east-directed Grasshopper Thrust (fig. 1; Ruppel and others, 1993) places Lemhi subbasin strata over the Mesoproterozoic eastern margin of the Lemhi subbasin (McDonald and Lonn, 2013). All pre-Tertiary rocks of the Salmon quadrangle are therefore allochthonous. Tertiary normal faults obscure the Grasshopper Thrust system along much of its length (McDonald and others, 2012) just as they complicate the other faults described above.

Muddy-Grasshopper Detachment and Other Normal Faults

Jänecke and others (1998, 1999, 2005; VanDenburg and others, 1998) describe the Muddy–Grasshopper Detachment as a shallowly west-dipping fault active from mid-Eocene to Oligocene times along the east edge of the Muddy Creek, Medicine Lodge, and Grasshopper basins and beneath the Horse Prairie subbasin. The Medicine Lodge beds were deposited during extension in an east-tilted half-graben, and sedimentation continued as younger normal faults dissected the half-graben, as detailed in VanDenburg and others (1998) and Jänecke and others (2005).

The Meriwether Lewis Fault zone is largely concealed. Stratigraphic offset does not require this to be a large fault zone, but Kickham (2002) estimates an offset of more than 5 km (3 mi). The numerous other Tertiary normal faults mapped in the Salmon quadrangle vary in strike from northwest to north to northeast, and can be either down-to-the-east or down-to-the–west.

Detrital Zircon Data (fig. 4)

Four detrital zircon samples of quartzite from the southeastern part of the quadrangle were collected and analyzed by Paul Link, Nathan Anderson, and Nick Krohe (written commun., 2016). Zircon U-Pb ages were obtained at the Arizona Laserchron Laboratory, with 100–106 grains analyzed per sample. Results are shown in figure 4 and appendix A, with sample locations shown on the geologic map (plate 1). Probability-frequency plots from all samples resemble published detrital zircon data from the Missoula Group and Lemhi strata (Link and others, 2016), with a major peak between 1,700 Ma and 1,730 Ma. Plots from 01NA15 and 02NA15 confirm their assignment to the Swauger Formation as shown on the geologic map. The plot for 03NA15 is also similar to Swauger Formation plots, but has been assigned to the Lawson Creek Formation based on its stratigraphic position above the chert-bearing zone at the base of the Lawson Creek Formation. Previously published detrital zircon data for the Lawson Creek Formation are few, but a plot from near the type section (Link and others, 2016) is similar to 03NA15. Three grains between 1,360 Ma and 1,400 Ma indicate that sample 03NA15 represents the youngest part of the Belt Supergroup, consistent with the stratigraphic position on the map.

Sample 05NA15 shows peaks at 1,721 Ma, 1,745 Ma, and 1,775 Ma, rather than a single sharp 1,720 Ma peak like the other three samples. Also in contrast to the other samples is the large percentage (17 percent) of Archean grains. Map relationships show sample 05NA15 to be from the Jahnke Lake member of the Apple Creek Formation even though it is coarser than is typical. The 1,775 Ma detrital zircon peak confirms its assignment. The coarse grains were likely derived from the nearby Dillon block, and they were probably also the source of the Archean ages. Other detrital zircon samples from this region also yielded significant Archean grains (Link and others, 2016; Sherwin and others, 2017).

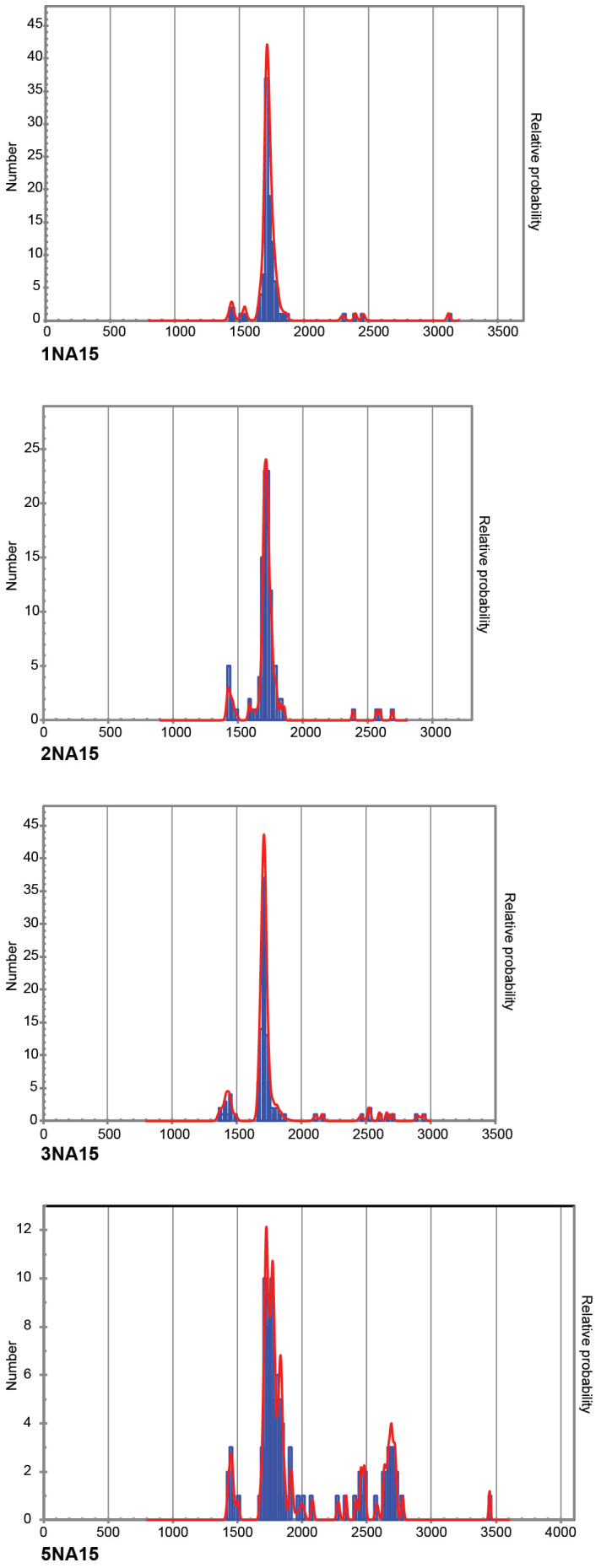

Figure 4. Detrital zircon U-Pb age spectra. Sample locations are shown on plate 1.

DESCRIPTION OF MAP UNITS

QUATERNARY, TERTIARY, AND MESOZOIC DEPOSITS

Qal **Alluvium (Holocene)**—Modern stream and floodplain deposits. As much as 100 m thick.

Qta **Talus and glacial deposits, undifferentiated (Holocene)**—Piles of angular boulders to cobbles on glaciated valley walls and in cirques. Mostly pro-talus ramparts, talus aprons, and slumps derived from moraine remnants and recent frost-wedged quartzite debris. Includes some alluvial fan gravel, and young glacial and periglacial deposits. Thickness less than 18 m (60 ft).

Qaf **Alluvial fan deposits (Holocene and Pleistocene)**—Subangular to subrounded, poorly sorted, cobble to boulder gravel, silt, and sand. Thickness unknown, but probably less than 60 m (200 ft).

Qalo **Older alluvium (Holocene and Pleistocene)**—Stream and floodplain deposits that are above the modern floodplain. Includes glacial outwash gravels, subrounded to rounded, well-sorted sandy cobble to boulder gravel and sand. Thickness unknown, but probably less than 150 m (490 ft).

Qls **Landslide deposits (Holocene and Pleistocene)**—Unsorted mixtures of silt, clay, sand, gravel and boulders. Typically characterized by hummocky topography. Not all mass wasting deposits are shown on the map because they are difficult to unambiguously identify.

Qlk **Lake deposits (Holocene and Pleistocene)**—Silt and sand deposited in standing water. Thickness 1–4 m (3–13 ft).

Qg **Glacial deposits, undivided (Holocene and Pleistocene)**—Most is unsorted, sandy to clayey, boulder to large boulder till with subangular to subrounded clasts. Also includes minor outwash, fan, kame, and esker deposits. Most till is probably of Pinedale age, but unit also includes younger glacial and periglacial deposits in higher elevations, and older till. There are older, partially dissected moraines located just west of Jackson, Montana. As thick as 100 m (330 ft).

Qc **Colluvial deposits (Holocene and Pleistocene)**—Mapped separately where so thick it completely masks the underlying deposits (Jänecke and others, 2005).

Qgr **Gravel (Holocene and Pleistocene)**—Thin pediment gravel deposits.

QTdf **Alluvial fan and debris flow fan deposits (Pleistocene to Tertiary)**—Subangular to subrounded, poorly sorted, boulder-cobble gravel, sand, and silt. Perched as much as 60 m above modern streams, but associated with modern drainages. Mapped in the northeastern part of the quadrangle. Thickness unknown.

QTgr **Gravel (Miocene or younger)**—Immature, unsorted, quartzite cobble gravel that may be colluvium or lag deposits from older gravel. No bedding or primary structures are visible. Forms aprons that slope away from highlands. May be equivalent to the Big Hole River Member of the Sixmile Creek Formation (Fritz and Sears, 1993). Thickness up to 60 m (200 ft).

Tbr **Breccia (Tertiary?)**—Area of angular quartzite clasts from pebble- to boulder-sized. Part of larger breccia field in the adjacent Ermont 7.5′ quadrangle (McDonald and Lonn, in review). Commonly lithified. Map pattern forms a half-circle around Black Mountain located along the border between the Ermont and west-adjacent Polaris 7.5′ quadrangles (Lonn and Lewis, 2012). Interpreted as a sedimentary debris flow or landslide deposit, but could be of tectonic origin. Unknown thickness.

Ts **Sediments, undifferentiated (Tertiary)**—Gravel, silt, sand, and clay. Red to pink, crudely bedded, poorly sorted, angular to subangular boulders, cobbles, pebbles and sand appear to overlie finer-grained sediments; otherwise there is no stratigraphic control. Thickness as much as 130 m (430 ft).

Tcl **Silt and clay (Miocene? to Eocene?)**—Light yellowish brown, massive silt and clay containing sparse matrix-supported pebbles and boulders. Typically capped by a flat surface of lag deposits containing subangular to subrounded

cobbles and boulders. Very poorly exposed. Thickness as much as 540 m (1,750 ft). Probably locally equivalent to the upper Medicine Lodge beds (Tml) of Jänecke and others (2005) but may correlate with Everson Creek (Tec) or Bannock Pass beds (Tbp).

Tgr **Fluvial gravel (late to middle Miocene)**—Mature gravel of well-rounded quartzite cobbles interlayered with varying amounts of fine-grained and ashy clastic sediments. Locally expressed as a lag deposit of cobbles. Appears to be the base of the Tertiary section where it rests on bedrock. In other places might be the Big Hole Member of the Sixmile Creek Formation elsewhere in southwest Montana (Fields and others, 1985; Fritz and Sears, 1993). Within the Grasshopper basin, mature gravel is interlayered with fine-grained lithic sandstone, siltstone, reworked tephra and ash, and mudstone that weathers to tan, buff and white, and is generally poorly exposed. Jänecke and others (2005) called these the Bannack (sic) Pass beds. Bedding and sedimentary structures are obscured by intense burrowing. Vertebrate fossils from correlative deposits at Bannock Pass in far southwest Montana are early to middle Miocene (M'Gonigle, 1994; Barnosky, 2001, 2007; Harris and others, 2017). At Bannock Pass, detailed tephrochronology places the base of Tsc at 21.4 Ma (Harris and others, 2017). Tabrum (in Nichols and others, 2001) identified fossils near Polaris as late Arikareean (North American Land Mammal age, ca. 18.5–23.0 Ma, after Barnosky and others, 2014). Thickness unknown.

Tec **Everson Creek beds (early Miocene to late Oligocene)**—Interbedded coarse sand, silt, and clay with minor conglomerate. Generally poorly exposed, but reflected by mottled uneven surfaces visible in aerial photographs. Areas underlain by Tec are oddly mottled and uneven in airphotos, which may reflect mass wasting, but also may reflect variation in lithification within the unit. Well-lithified sandstone and conglomerate channels running through the soft, poorly lithified, muddy sediments that make up the bulk of Tec may also account for the unusual surface features. Distinctive, well-cemented lenses of two-mica-bearing feldspathic sandstone and conglomerate have trough to planar cross beds and well-developed pebble imbrications. Lenses are interpreted to be fluvial channel deposits within overbank muds (Thomas, 1995; Roe, 2010; Barber, 2013). Vertebrate fossils from correlative units in the Everson Creek 7.5′ quadrangle to the south indicate a late early Arikareean age (Nichols and others, 2001; North American Land Mammal age, ca. 29.5–25.0 Ma, after Barnosky and others, 2014).

Tls **Paleolandslide deposits (Oligocene and/or Eocene)**—Unsorted hummocky deposits and large slide blocks. Composition typically reflects quartzites of the immediate source area, but locally includes both intact and brecciated masses of Challis Volcanic Group clasts (Jänecke and others, 2005). Locally interbedded with Medicine Lodge beds (Tml and Tmlc). Jänecke and others (2005) describe slide blocks up to 2 km long (1.2 mi), including a large block of maroon quartzite that now makes up Red Butte in the southeast corner of the map area. They describe the quartzite as belonging to the Missoula Group of the Belt Supergroup, but it is more likely to be from the Swauger Formation. Jänecke and others (2005) interpret Tls deposits as having slid from the west into the Grant protobasin during extension on the shallowly west-dipping Muddy–Grasshopper Detachment. However, Lonn interprets these exposures as para-autochthonous bedrock knobs protruding through the Cenozoic deposits, developed by pre- or early Tertiary erosion.

Tml **Medicine Lodge beds and equivalents (late Oligocene to Eocene)**—Basin-fill deposits described in detail by Jänecke and others (2005). Includes a wide variety of clastic sediments that grade laterally over short distances from conglomerate to feldspathic and quartzose sandstones, shale, and mudstone. Sediments are commonly tuffaceous. Sandstones are typically lenticular and cross-bedded. Fossils and $^{40}Ar/^{39}Ar$ dates for volcanic components (summarized in table 1 of Jänecke and others, 2005) support the conclusion that the Medicine Lodge beds are equivalent in age to the Renova Formation elsewhere in Montana. Thickness over 1,000 m (3,300 ft) in the southeast corner of the map.

Tmlc **Medicine Lodge beds conglomerate (Oligocene to Eocene)**—Angular to rounded, quartzite cobble conglomerate and angular to rounded cobble float that is locally well cemented. Composed of alluvial, fluvial, and debris flow deposits generally derived from Proterozoic rocks of adjacent highlands, though conglomerates on the farthest east were derived from Paleozoic and Mesozoic rocks in the footwall of the Muddy–Grasshopper Detachment (Jänecke and others, 2005). As thick as 550 m (1,800 ft).

TKb **Beaverhead Group (Tertiary? and Cretaceous)**—Massive boulder-cobble conglomerate containing mostly Proterozoic quartzite and Paleozoic limestone clasts. In contrast to Tertiary conglomerates, it is complexly folded and well indurated. Occurs in the footwall of a thrust fault along the southeastern border of the quadrangle.

PALEOZOIC STRATA

A poorly exposed and incomplete Middle Cambrian to Pennsylvanian section is present in the northeastern part and along the central eastern border of the Salmon quadrangle. A fault system at a low angle to bedding omits various Cambrian units. This bedding-parallel fault system is very similar to one in the northern Pioneer Mountains that also tectonically thins the lower Paleozoic section (McDonald and others, 2012).

IPq **Quadrant Formation (Pennsylvanian)**—Light gray, pinkish gray, and yellowish gray, medium- to thick-bedded, medium- to fine-grained, well-sorted, quartz sandstone with rounded grains cemented by quartz overgrowths. Very light gray, medium to thick dolomite beds may be present in the lowermost and uppermost parts, interbedded with quartz sandstone. Occurs as brecciated masses associated with complex faulting in the easternmost part of the quadrangle.

Mm **Madison Group, undivided (Mississippian)**—Mostly Mission Canyon Limestone: Gray, microcrystalline, thick-bedded locally fossiliferous limestone with abundant gray, black, olive, and pale yellowish brown lentil-shaped or elongate chert nodules. Includes some Lodgepole Limestone: Dark gray, thin-bedded, microcrystalline limestone, with yellowish brown and grayish orange, thin partings and interbeds of calcareous mudstone. Exposed only on a thrust plate in the southeastern part of the map. Thickness unknown.

Dj **Jefferson Formation (Devonian)**—Dark gray, yellow, and white, sugary dolomite and limestone. Commonly bleached and recrystallized to white marble. Dark gray dolomite distinguishes this unit from the lighter-colored Hasmark Formation (unit Ꞓh). Strongly deformed, with numerous intraformational faults, abundant tectonic breccia, and tight folds. Deformation makes thickness estimates problematic, but probably more than 300 m (980 ft) thick.

Ꞓrl **Red Lion Formation (Cambrian)**—Multicolored and lithologically variable unit that includes red dolomite with thin maroon anastomosing shaly layers, shaly conglomerate containing limestone and mud-chip intraclasts, reddish calcareous silty shale, and calcareous and non-calcareous sandstone and quartzite. Thickness approximately 40 m (130 ft).

Ꞓh **Hasmark Formation (Cambrian)**—Light gray to white, thinly laminated to massive dolomite with minor magnesium limestone intervals. Weathers very light gray with a smooth, laminated surface. Thickness as much as 100 m (330 ft).

Ꞓq **Quartzite (Cambrian)**—Dense, white, moderately well-sorted, fine- to medium-grained quartzite. Bedding difficult to see. Contains 96–99 percent quartz, 1–2 percent plagioclase, no potassium feldspar, and 1 percent red chert and black hematite grains. Also contains sparse coarse floating grains of well-rounded quartz. Interpreted to lie above or within the upper part of the Silver Hill Formation. Similar quartzite occupies an identical stratigraphic position near Argenta, 10 km (6 mi) east of the map area, where it is gradational with underlying micaceous shale (McDonald and Lonn, in review).

Ꞓsh **Silver Hill Formation (Cambrian)**—Lithologically varied unit. Very poorly exposed, but contains brown to greenish brown micaceous shale, distinctive red to maroon argillite and siltite, dark gray limestone with wavy yellow-

brown silty seams that impart a "black and gold" color to rock, calcareous sandstone, white, feldspar-poor quartzite, and quartz-pebble conglomerate. Thickness as much as 105 m (345 ft).

Cf **Flathead Formation (Cambrian)**—Dense, hard, pink, white, or salmon, medium- to coarse-grained, moderately sorted, thick-bedded, feldspar-poor quartzite with prominent crossbeds, although locally the laminations are faint. Contains massive beds up to 1 m (3 ft) thick. Most grains are rounded to subrounded. Contains rare granules and small rounded pebbles of quartzite, quartz, and red chert. Contains 89–97 percent quartz, no potassium feldspar, 0–3 percent plagioclase, up to 3 percent red chert (?) grains and up to 11 percent interstitial sericite and other unidentified interstitial minerals. Occurs in the northeastern part of the quadrangle where it overlies Swauger Formation or Lawson Creek Formation. Thickness varies from less than 200 m (660 ft) near Jackson to more than 600 m (2,000 ft) on the eastern edge of the quadrangle. While these thicknesses appear atypical for Flathead Formation, in the east adjacent Ermont 7.5′ quadrangle (McDonald and Lonn, in review), it was estimated to be 600 m (2,000 ft) thick, and McDonald (in review) reports an estimated thickness of 305 m (1,000 ft) in nearby areas. The contact with underlying Mesoproterozoic units is a low-angle unconformity that is difficult to pinpoint.

MESOPROTEROZOIC STRATA

Our new mapping shows that >4,500 m (14,800 ft) of Mesoproterozoic strata rest on top of the previously described Lemhi Group and overlying Swauger and Lawson Creek Formation (Ruppel, 1975; Hobbs, 1980; Burmester and others., 2013, 2016a; fig. 1). We now refer to the Lemhi Group plus the strata above it—Swauger, Lawson Creek, and Apple Creek Formations—as the Lemhi subbasin strata. These strata, which are sandier than typical Belt units, extend north and northeast into Montana where they grade into the Missoula Group of the upper Belt Supergroup (fig. 2; Lonn, 2014; Lonn and others, 2016a,b).

The MBMG-IGS collaborative team now assigns all Proterozoic strata in the Salmon quadrangle to the Lemhi subbasin section (Burmester and others, 2013, 2016a,b, 2017). However, the thicknesses and lithologies of the Swauger Formation, Lawson Creek Formation, and Jahnke Lake member of the Apple Creek Formation change considerably from the western to the eastern and northern sides of the quadrangle. The Jahnke Lake member is unrecognized northeast of the Buffalo Creek–Jackson Fault Zone, where Cambrian strata disconformably overlie a thick section of Lawson Creek Formation. Eastward changes in grain size and thicknesses in the Swauger Formation, the Lawson Creek Formation, and the Jahnke Lake member (described below) could be the result of facies changes near the eastern margin of the Lemhi subbasin, or they could result from miscorrelation of the argillite-rich intervals used to divide the formations within this immensely thick quartzite succession. The Gunsight Formation is also coarser grained and thicker bedded to the east in the footwall of the Freeman–North Fork Thrust than it is in the hanging wall near the western border of the map. This may be the result of the proximity of the Belt Basin margin immediately east of the map, or it may because the western facies has been miscorrelated (see discussion below).

Yaj **Jahnke Lake member, Apple Creek Formation (Mesoproterozoic)**—Gray, pale green or light red to pink, thick-bedded, very fine- to medium-grained, well-sorted, very feldspathic quartzite. In the west, bedding is difficult to see, but where visible is commonly defined by dark laminations rich in hematite grains. Convolute bedding resulting from soft sediment deformation is common. Thin skins of green argillite commonly separate the meter-scale quartzite beds, and thin mud rip-ups are present but uncommon. Rare chert rip-ups are also present. Toward the east, the rocks are less metamorphosed, bedding is well-defined, and small red mud chips are locally abundant. Feldspar content ranges from 20 percent to 50 percent, with plagioclase more abundant than potassium feldspar in the west, subequal in the east. The unit is correlated with the lowest part of the redefined Apple Creek Formation in the Lemhi Range to the southwest (Burmester and others, 2013, 2016a,b). Best exposed on the ridge north of Jahnke Lake on the Goldstone Pass 7.5′ quadrangle (Lonn and others, 2009). Thickness ranges from 0 m near Jackson in the northeast-

ern part of the quadrangle to 4,300 m (14,000 ft) in the hanging wall of the Eastern Strand of the Beaverhead Divide Fault, where the upper contact is not exposed and the lower contact is gradational with the underlying Lawson Creek Formation.

Ylc **Lawson Creek Formation (Mesoproterozoic)**—Characterized by couplets (centimeter-scale alternating beds) and couples (decimeter-scale alternating beds) of fine- to medium-grained white quartzite alternating with purple, black, and green argillite. Lenticular and flaser bedding are common and characteristic. Mud rip-up clasts are locally common, and some are very large, as much as 15 cm in diameter; chert beds and cherty rip-up clasts are less common. The thick section on the eastern part of the quadrangle is dominated by thick intervals of fine- to medium-grained, relatively quartz-rich (up to 90 percent) quartzite separated by thinner argillite-rich intervals. In the western part of the map, the lower contact is placed at the bottom of the thin-bedded, argillite-rich interval that gradationally overlies the coarse-grained Swauger Formation, and the upper contact is placed at the top of the uppermost argillite-rich strata beneath the dominantly thick-bedded, fine-grained quartzite of the Jahnke Lake member of the Apple Creek Formation. In the eastern part of the map, northeast of the Buffalo Creek–Jackson Fault Zone, the lower contact is placed at the lowest occurrence of chert rip-up clasts above the coarse-grained Swauger Formation and the upper contact is not exposed. Not identified along the eastern border of the map where Cambrian sediments overlie Swauger Formation. Thickness where identified varies from 300 m (980 ft) in the Beaverhead Mountains to 2,150 m (7,000 ft) on the east side of the Buffalo Creek–Jackson Fault. The detrital zircon data presented above suggest that the large difference in thicknesses is due to facies changes across the Buffalo Creek–Jackson Fault, with the upper part of the Lawson Creek northeast of the fault being time-correlative with the Jahnke Lake member southwest of the fault. The Lawson Creek Formation is tentatively correlated with the McNamara Formation of the Missoula Group, Belt Supergroup, on the basis of similar lithology and stratigraphic position.

Ysw **Swauger Formation (Mesoproterozoic)**—Red, pink, and white, poorly sorted, medium- to coarse-grained, trough and planar cross-bedded quartzite in beds as thick as 2 m (6 ft). Contains small pebbles, black or purple mudcracked argillite beds as thick as 2 cm, thick black mud rip-up clasts, and coarse, floating, well-rounded quartz grains. Chalky white feldspar grains are obvious in hand sample. Feldspar content ranges from 10 to 40 percent with potassium feldspar dominant over plagioclase. Lower part is very coarse and contains pebbles as large as 5 cm in diameter of well-rounded quartzite and angular quartz and feldspar. Grades downward into the Gunsight Formation (Ygs), and upward into Lawson Creek Formation (Ylc). Best exposed section is on the ridge north of Miner Creek in the Homer Youngs Peak 7.5′ quadrangle (Lonn and others, 2008) in the Beaverhead Mountains. Thickness varies from 5,500 m (18,000 ft) in the Beaverhead Mountains to 2,770 m (9,100 ft) northeast of the Jackson Fault Zone. As with the Lawson Creek Formation, this thickness variation could be due to lateral facies changes or to miscorrelation of the argillite-rich intervals that separate the Swauger from the overlying Lawson Creek. The Swauger Formation is tentatively correlated with the Bonner and Mount Shields Formations of the Missoula Group, Belt Supergroup, on the basis of lithologic similarity and stratigraphic position.

Ygs **Gunsight Formation (Mesoproterozoic)**—Northeast of the North Fork Thrust, Gunsight Formation is observed in stratigraphic contact with the overlying Swauger Formation. Here, Gunsight is mostly gray, pale green, or light red, moderately well-sorted, fine-grained, very feldspathic quartzite characterized by flat laminations of black hematite; typically weathers into thick (8 cm) plates. Contains some crossbeds and minor thin argillite layers that are commonly mudcracked. Near the top, includes thin layers of coarse, well-rounded quartz grains interpreted to be lag deposits. Feldspar content is 35 to 40 percent, with plagioclase and potassium feldspar in subequal amounts. Upper contact is

gradational with the overlying Swauger Formation (Ysw). Only the upper 770 m (2,500 ft) is exposed northeast of the North Fork Thrust.

Southwest of the North Fork Thrust, in its hanging wall, Gunsight Formation (labeled Ygs?) is thinner bedded and finer-grained, consisting of interbedded intervals of couplets (centimeter-scale beds) of dark siltite grading up to darker gray to green argillite, and couples (decimeter-scale beds) of white, very fine-grained, very feldspathic quartzite grading up to dark-colored silt. Thicker beds typically have bedding defined by dark millimeter-scale flat laminations. Load casts, convolute lamination, and decimeter-thick stacks of centimeter-scale ripple cross lamination are also common. Coarser, quartzite-rich intervals appear to be laterally discontinuous. Thickness uncertain because of deformation, but a minimum of 2,400 m (7,900 ft) is likely. Unit Ygs? is fault bounded, and therefore its stratigraphic position is unknown. Although originally correlated with Gunsight Formation (Burmester and others, 2016a), recent work outside the quadrangle has called this interpretation into question (Burmester and others, 2017). In addition, a single detrital zircon grain from this unit immediately south of the Salmon quadrangle yielded a 1,373 Ma age (Gillerman, 2008), suggesting the unit is near the top of the Lemhi section (Apple Creek) rather than near the bottom (Gunsight Formation). Unit Ygs? may therefore be correlative with part of the Apple Creek Formation.

Yyb? **Yellow Lake and Big Creek Formations, undivided (Mesoproterozoic)**—Quartzite, siltite, and argillite that are commonly carbonate bearing and locally phyllitic. Unit Yyb? occurs in the structural domain between the Freeman and North Fork Thrusts in the Beaverhead Range, where complex internal faulting, folding, and strong cleavage prevent separation of individual formations. Big Creek Formation is mostly greenish, calcareous coarse siltite in meter-thick beds. Yellow Lake Formation gradationally overlies Big Creek, and is mostly phyllitic dark-colored siltite and argillite couplets (centimeter- to millimeter-scale), with locally abundant carbonate and pinch-and-swell bedforms. Complex structure precludes thickness estimates, but together these formations are at least 2,800 m (9,200 ft) thick in their type sections in the Lemhi Range (Ruppel, 1975; Lonn, 2017).

Similar lithologies in the North Fork area northwest of this map (Burmester and others, 2016a) have recently been reinterpreted as the banded siltite member of the Apple Creek Formation because diamictite was observed (Burmester, Lewis, Lonn, unpublished mapping, 2017) and diamictite has been reported only in members of the Apple Creek Formation (Tietbohl, 1986; Connor and Evans, 1986; Tysdal, 2000). Therefore, an alternative interpretation is that this unit (Yyb?) also correlates with the banded siltite member of the Apple Creek Formation.

Xgbd **Gneiss of Bloody Dick Creek (Paleoproterozoic)**—Finely layered biotite gneiss with zones of medium-grained augen gneiss, felsic gneiss, and hornblende gneiss. Biotite schist occurs within all gneisses. Primary mineralogy is quartz, plagioclase, biotite, and hornblende, with minor garnet and altered pyroxene (Coppinger, 1974). Pearson and others (2017), using zircon U-Pb and Lu-Hf analysis, postulated a 2,438 Ma protolith was intruded at 1,802 Ma and metamorphosed at 1,759 Ma. They proposed that all rocks had an igneous protolith. Richard Gaschnig (written commun., 2009) reported similar ages: about 1,800 Ma for metamorphism and 1,830 Ma for the youngest non-metamorphic zircons (Sherwin and others, 2017). Numerous centimeter- to meter-thick quartz veins occur throughout the unit and are associated with gold–silver–copper–lead mineralization (Brenner-Younggren and Cox, 2017).

IGNEOUS ROCKS

Intrusive rocks extensively exposed in the northeastern part of the quadrangle are part of the Pioneer Batholith. A smaller composite stock, the Carmen Creek Stock, crops out in the westernmost part of the map area and has apparently intruded an east–west structure interpreted as a down-to-the-south normal fault. Eocene diorite dikes are scattered across the quadrangle and locally intrude fault zones; some are

strongly deformed and interpreted to record Eocene or later faulting.

Tba **Basalt (Oligocene)**—Rusty brown weathering, dark gray, aphanitic, vesicular, and amygdaloidal basalt flows in the eastern part of the quadrangle. Matoush (2002), Kickham (2002), and Jänecke and others (2005) reported four nearly identical $^{40}Ar/^{39}Ar$ ages of 27–28 Ma for erosional remnants of these basalt flows and shallow intrusions. This valley-filling basalt has impressive colonnades of cooling joints southwest of Bannack, Montana. Some dikes are also present in the underlying Medicine Lodge beds but extrusive masses are more common than intrusive ones. Tba is in the western edge of the 53–17 Ma Dillon Volcanic field of Fritz and others (2007).

Tdi **Diorite dikes (Eocene)**—Dark-colored, fine- to medium-grained hornblende diorite. Mostly occurs as dikes that may be undeformed, have sheared margins, or be strongly foliated. One dike in the Goldstone Pass 7.5′ quadrangle (Lonn and others, 2009) of the central Beaverhead Range has a U-Pb zircon age of 46 Ma (Richard Gaschnig, written commun., 2009). Where deformed, these dikes record Eocene or later faulting.

Tgd **Granodiorite (Eocene)**—Hornblende–biotite granodiorite of the Carmen Creek Stock in the westernmost part of the quadrangle. Complexly zoned oligoclase ($An_{25–35}$), quartz, microcline, hornblende, and biotite are the major constituents (MacKenzie, 1949; Anderson, 1959; Kilroy, 1981). Eocene age based on $^{40}Ar/^{39}Ar$ dating of biotite (47.7 ± 0.6 Ma and 49.4 ± 0.8 Ma) and hornblende (50.5 ± 1.8 Ma; Kilroy, 1981), and a U-Pb zircon age of 49.2 ± 1.7 Ma (Darin Schwartz, written commun., 2011).

TKgd **Granodiorite (Tertiary or Cretaceous)**—White, equigranular, biotite–hornblende granodiorite. Composition typically 60 percent plagioclase, 23 percent quartz, 9 percent biotite, 3 percent hornblende, 2 percent potassium feldspar, and 3 percent accessory minerals including sphene, apatite, zircon, and pyrite (Coppinger, 1974).

TKv **Volcanic rocks, undivided (Tertiary or Cretaceous)**—Gray, hornblende porphyry and white to red lithic tuff containing round quartz grains. Poorly exposed on the eastern edge of the quadrangle. Mosolf (in review) reported late Cretaceous U-Pb zircon ages for similar volcanic rocks in the east-adjacent Bannack 7.5′ quadrangle.

Kdi **Diorite (Cretaceous?)**—Hornblende diorite of the Carmen Creek Stock in the westernmost part of the quadrangle. Composed of 50–75 percent hornblende along with plagioclase, hypersthene, actinolite, quartz, and opaque minerals, and also contains small hornblende pyroxenite xenoliths (Kilroy, 1981).

Kgdp **Porphyritic granodiorite (Cretaceous)**—Porphyritic biotite granodiorite of the Pioneer Batholith. Contains phenocrysts of potassium feldspar as large as 6 cm. Hornblende is absent (Berger and others, 1983).

Kgd **Granodiorite (Cretaceous)**—Light gray, massive, medium-grained, hornblende–biotite granodiorite of the Pioneer Batholith in the northeastern part of the quadrangle. Locally contains large potassium feldspar phenocrysts up to 2 cm long (Pearson and Zen, 1985; Zimbelman, 1984). Equivalent to the Uphill Creek granodiorite of Pearson and Zen (1985), the predominant rock type of the Pioneer Batholith. Best age estimate of the unit is an $^{40}Ar/^{39}Ar$ date of 75 Ma (Snee, 1982).

Kgb **Hornblende gabbro (Cretaceous)**—Medium to dark gray, medium- to coarse-grained, hypidiomorphic granular hornblende gabbro containing an average 40–45 percent plagioclase, 45–55 percent hornblende after augite, 3–5 percent augite cores in hornblende, and 0–5 percent biotite (Zimbelman, 1984; Pearson and Zen, 1985). Age determined through U-Pb dates is 70–72 Ma (Katie McDonald, written commun.). Thought to be an early border phase of the Pioneer Batholith (Snee, 1982; Zimbelman, 1984).

Kqd **Quartz diorite (Cretaceous)**—Biotite–hornblende quartz diorite of the Carmen Creek Stock in the westernmost part of the map area. Composed of 45–55 percent andesine ($An_{40–50}$)

along with hornblende, biotite, quartz, and orthoclase (Kilroy, 1981). Cretaceous age based on $^{40}Ar/^{39}Ar$ hornblende dates of 81.5 ± 1.6 Ma and 80.3 ± 2.2 Ma, which are considered to be minimum ages for this unit (Kilroy, 1981).

REFERENCES

Anderson, A.L., 1959, Geology and mineral resources of the North Fork quadrangle, Lemhi County, Idaho: Idaho Bureau of Mines and Geology Pamphlet 118, 92 p.

Barber, D.E., 2013, Implications for tectonic control on paleogeography and sediment dispersal pathway: Integrated U-Pb detrital zircon age-analysis of the Paleogene Missouri River headwater system, SW Montana: Meadville, Pennsylvania, Allegheny College, B.S. thesis, 149 p.

Barnosky, A.D., 2001, Distinguishing the effects of the Red Queen and Court Jester on Miocene mammal evolution in the northern Rocky Mountains: Journal of Vertebrate Paleontology, v. 21, p. 172–185, doi: 10.1671/0272-4634(2001)021[0172:DTEOTR]2.0.CO;2.

Barnosky, A.D., Bibi, F., Hopkins, S.S.B., and Nichols, R., 2007, Biostratigraphy and magnetostratigraphy of the mid-Miocene Railroad Canyon sequence, Montana and Idaho, and age of the mid-Tertiary unconformity west of the Continental Divide: Journal of Vertebrate Paleontology, v. 27, p. 204–224, doi: 10.1671/0272-4634(2007)27.

Barnosky, A.D., Holmes, M., Kirchholtes, R., Lindsey, E., Maguire, K.C., Poust, A.W., Stegner, M.A., Sunseri, J., Swartz, B., Swift, J., Villavicencio, N.A., and Wogan, G.O.U., 2014, Prelude to the Anthropocene: Two new North American Land Mammal Ages (NALMAs): The Anthropocene Review, v. 1, p. 225–242.

Berger, B.R., Snee, L.W., and Hanna, William, 1983, Mineral resource potential of the West Pioneer wilderness study area, Beaverhead County, Montana: U.S. Geological Survey Miscellaneous Field Studies Map MF-1585, scale 1:50,000.

Brenner-Younggren, E., and Cox, B.E., 2017, Lithologic and structural controls of mineral deposits in the Horse Prairie basin, Beaverhead County, Montana, with notes on Horse Prairie history: Northwest Geology, v. 46, p. 143–152.

Burmester, R.F., Lewis, R.S., Othberg, K.L., Lonn, J.D., Stanford, L.R., and McFaddan, M.D., 2011, Geologic map of the Badger Spring Gulch quadrangle, Lemhi County, Idaho: Idaho Geological Survey Digital Web Map 132, scale 1:24,000.

Burmester, R.F., Lonn, J.D., Lewis, R.S., and McFaddan, M.D., 2013, Toward a grand unified theory for stratigraphy of the Lemhi subbasin of the Belt Supergroup: Northwest Geology, v. 42, p. 1–20.

Burmester, R.F., Lewis, R.S., Othberg, K.L., Stanford, L.R., Lonn, J.D., and McFaddan, M.D., 2016a, Geologic map of the western part of the Salmon 30′ x 60′ quadrangle, Idaho and Montana: Idaho Geological Survey Geologic Map 52, scale 1:75,000.

Burmester, R.F., Lonn J.D., Lewis, R.S., and McFaddan, M.D., 2016b, Stratigraphy of the Lemhi subbasin of the Belt Supergroup, in MacLean, J.S., and Sears, J.W., eds., Belt Basin: Window to Mesoproterozoic Earth: Geological Society of America Special Paper 522, p. 1–29, doi:10.1130/2016.2522(05).

Burmester, R.F., Lewis, R.S., and Lonn J.D., 2017, Were we wrong? Second thoughts on the geology of the Lemhi subbasin: Northwest Geology, v. 46, p. 7–14.

Connor, J.J., and Evans, K.V., 1986, Geologic map of the Leesburg quadrangle, Idaho: U.S. Geological Survey Miscellaneous Field Studies Map MF-1880, scale 1:62,500.

Coppinger, Walter, 1974, Stratigraphy and structural study of Belt Supergroup and associated rocks in a portion of the Beaverhead Mountains, southwestern Montana and east-central Idaho: Oxford, Ohio, Miami University, Ph.D. dissertation, 224 p.

Elliott, C.G., and Lonn, J.D., 2016, Geologic map of the Tash Peak 7.5' quadrangle, southwest Montana: Montana Bureau of Mines and Geology Open-File Report 678, scale 1:24,000.

Elliott, C.G., and Lonn, J.D., 2017, Walking tour of the Monument Fault near the confluence of Bloody Dick Creek and Horse Prairie Creek, southwestern Montana: Northwest Geology v. 46, p. 113–118.

Fields, R.W., Rasmussen, D.L., Tabrum, A.R., and Nichols, R., 1985, Cenozoic rocks of the inter-

montane basins of western Montana and eastern Idaho; a summary, in Flores, R.M., and Kaplan, S.S., eds., Cenozoic paleogeography of the west-central United States: Society of Economic Paleontologists and Mineralogists, Rocky Mountain Section, Rocky Mountain Paleogeography Symposium, v. 3, p. 9–36.

Fritz, W.J., and Sears, J.W., 1993, Tectonics of the Yellowstone hotspot wake in southwestern Montana: Geology, v. 21, p. 427–430.

Fritz, W.J., Sears, J.W., McDowell, R.J., and Wampler, J.M., 2007, Cenozoic volcanic rocks of southwestern Montana, in Thomas, R.C., and Gibson, R.I., eds., Dillon, Montana: Tobacco Root Geological Society 32nd Annual Field Conference Guidebook, Northwest Geology, v. 36, p. 91–110.

Gillerman, V.S., 2008, Geochronology of iron oxide-copper-thorium-REE mineralization in Proterozoic rocks at Lemhi Pass, Idaho, and a comparison to copper-cobalt ores, Blackbird Mining District, Idaho: Final Technical Report to U.S. Geological Survey, Grant Award 06HQGR0170, 66 p.

Harris, E.B., Strömberg, C.A.E., Sheldon, N.D., Smith, S.Y., and Ibañez-Mejia, M., 2017, Revised chronostratigraphy and biostratigraphy of the early-middle Miocene Railroad Canyon section of central-eastern Idaho, USA: Geological Society of America Bulletin, v. 129, p. 1241–1251, doi: 10.1130/B31655.1.

Harrison, J.E., and Cressman E.R., 1993, Geology of the Libby thrust belt of northwestern Montana and its implications to regional tectonics: U.S. Geological Survey Professional Paper 1524, 42 p., map scale 1:125,000.

Hobbs, S.W., 1980, The Lawson Creek Formation of Middle Proterozoic age in east-central Idaho: U.S. Geological Survey Bulletin 1482-E, 12 p.

Jänecke, S.U., 1994, Sedimentation and paleogeography of an Eocene to Oligocene rift zone, Idaho and Montana: Geological Society of America Bulletin, v. 106, p. 1083–1095.

Jänecke, S.U., 2007, Cenozoic extensional processes and tectonics in the northern Rocky Mountains: Northwest Geology, v. 36, p.111–132.

Jänecke, S.U., Blankenau, J.J., VanDenburg, C.J., and Van Gosen, B.S., 2001, Normal faults and extensional folds of southwest Montana and eastern Idaho: Geometry, relative ages, and tectonic significance: U.S. Geological Survey Miscellaneous Field Studies 2362, scale 1:100,000.

Jänecke, S.U., Dorsey, R.J., Kickam, J.C., Matoush, J.P., and McIntosh, W.C., 2005, Geologic map of the Bachelor Mountain 7.5' quadrangle, southwest Montana: Montana Bureau of Mines and Geology Open-File Report 525, 27 p., scale 1:24,000.

Jänecke, S.U., McIntosh, W., and Good, S., 1999, Testing models of rift basins—Structure and stratigraphy of an Eocene–Oligocene supradetachment basin, Muddy Creek half graben, southwest Montana: Basin Research, v. 11, no. 2, p. 143–167.

Jänecke, S.U., VanDenburg, C. J., and Blankenau, J. J., 1998, Geometry, mechanisms, and significance of extensional folds from examples in the Rocky Mountain Basin and Range province, U.S.A.: Journal of Structural Geology, v. 20, p. 841–856.

Jänecke, S.U., VanDenburg, C.J., Blankenau, J.J., and M'Gonigle, J.W., 2000, Long-distance longitudinal transport of gravel across the Cordilleran thrust belt of Montana and Idaho: Geology, v. 28, no. 5, p. 439–442.

Kickham, J.C., 2002, Structural and kinematic evolution of the Grasshopper extensional basin, southwest Montana: Logan, Utah State University, M.S. thesis, 141 p.

Kilroy, K.C., 1981, 40Ar/39Ar geochronology and geochemistry of the Carmen Creek Stock, and related intrusions of the northern Beaverhead Mountains, Idaho–Montana: Columbus, Ohio State University, M.S. thesis, 100 p.

Lewis, R.S., Burmester, R.F., Stanford, L.R., Lonn, J.D., McFaddan, M.D., and Othberg, K.L., 2009a, Geologic map of the Kitty Creek 7.5' quadrangle, Lemhi County, Idaho, and Beaverhead County, Montana: Montana Bureau of Mines and Geology Open-File Report 582, scale 1:24,000.

Lewis, R.S., Burmester, R.F., Stanford, L.R., Lonn, J.D., McFaddan, M.D., and Othberg, K.L., 2009b, Geologic map of the Bohannon Spring 7.5' quadrangle, Lemhi County, Idaho, and Beaverhead County, Montana: Montana Bureau of Mines and Geology Open-File Report 583, 1 sheet, scale 1:24,000.

Lewis, R.S., Othberg, K.L., Lonn, J.D., Burmester, R.F., McFaddan, M.D., and Stanford, L.R., 2011, Geologic map of the Goldstone Mountain 7.5' quadrangle, Montana and Idaho: Montana Bureau of Mines and Geology Open-File Report 604, scale 1:24,000.

Link, P.K., Stewart, E.D., Steel, T., Sherwin, J., Hess, L.T., and McDonald, C., 2016, Detrital zircons in the Mesoproterozoic upper Belt Supergroup in the Pioneer, Beaverhead, and Lemhi Ranges, Montana and Idaho: The Big White arc, in MacLean, J.S., and Sears, J.W., eds., Belt Basin: Window to Mesoproterozoic Earth: Geological Society of America Special Paper 522, doi:10.1130/2016.2522(07).

Lonn, J.D., 2014, The northern extent of the Mesoproterozoic Lemhi Group, Idaho and Montana, and stratigraphic and structural relations with Belt Supergroup strata: Geological Society of America Abstracts with Programs, v. 46, no. 5, p. 72.

Lonn, J.D., 2017, The Lemhi Group type section revisited and revised, east-central Idaho: Northwest Geology, v. 46, p. 15–28.

Lonn, J.D., and Lewis, R.S., 2011, Geologic map of the Peterson Lake 7.5' quadrangle, southwestern Montana: Montana Bureau of Mines and Geology Open-File Report 606, scale 1:24,000.

Lonn, J.D., and Lewis, R.S., 2012, Geologic map of the Polaris 7.5' quadrangle, southwestern Montana: Montana Bureau of Mines and Geology Open-File Report 621, scale 1:24,000.

Lonn, J.D., and McDonald, C., 2004, Geologic map of the Kelly Lake 7.5' quadrangle, western Montana: Montana Bureau of Mines and Geology Open-File Report 500, 15 p., scale 1:24,000.

Lonn, J.D., Skipp, B., Ruppel, E.T., Jänecke, S.U., Perry, W.J., Jr., Sears, J.W., Bartholomew, M.J., Stickney, M.C., Fritz, W.J., Hurlow, H.A., and Thomas, R.C., 2006 (revised), Geologic map of the Lima 30' x 60' quadrangle, southwest Montana: Montana Bureau of Mines and Geology Open-File Report 408, scale 1:100,000.

Lonn, J.D., Burmester, R.F., Lewis, R.S., and Stanford, L.R., 2008, Geologic map of the Homer Youngs Peak quadrangle, Lemhi County, Idaho, and Beaverhead County, Montana: Idaho Geological Survey Digital Web Map 95 and Montana Bureau of Mines and Geology Open-File Report 575, scale 1:24,000.

Lonn, J.D., Stanford, L.R., Burmester, R.F., Lewis, R.F., and McFaddan, M.D., 2009, Geologic map of the Goldstone Pass 7.5' quadrangle, Lemhi County, Idaho, and Beaverhead County, Montana: Montana Bureau of Mines and Geology Open-File Report 584, scale 1:24,000.

Lonn, J.D., Burmester, R.F., McFaddan, M.D., and Lewis, R.S., 2011, Geologic map of the Selway Mountain 7.5' quadrangle, Beaverhead County, Montana: Montana Bureau of Mines and Geology Open-File Report 598, scale 1:24,000.

Lonn, J.D., Othberg, K.L., Lewis, R.S., Burmester, R.F., Stanford, L.R., Stewart, D.E., and Freed, J.S., 2013, Geologic map of the North Fork quadrangle, Lemhi County, Idaho: Idaho Geological Survey, DMW-160, scale 1:24,000.

Lonn, J.D., Lewis, R.S., Burmester, R.F., and McFaddan, M.D., 2013b, Geologic map of the Jumbo Mountain 7.5' quadrangle, southwestern Montana and east-central Idaho: Montana Bureau of Mines and Geology Open-File Report 634, scale 1:24,000.

Lonn, J.D., Lewis, R.S., Burmester, R.F., and McFaddan, M.D., 2013c, The complex structural geology of the northern Beaverhead Mountains, Montana and Idaho: Northwest Geology, v. 42, p. 111–130.

Lonn, J.D., Lewis, R.S., Burmester, R.F., and McFaddan, M.D., 2016a, Mesoproterozoic Lemhi strata represent immense alluvial aprons that prograded northwest into the Belt Sea, Idaho and Montana: Geological Society of America Rocky Mountain Section Meeting, Moscow, Idaho: https://gsa.confex.com/gsa/2016RM/webprogram/Paper276082.html

Lonn J.D., Burmester, R.F., Lewis, R.S. , and McFaddan, M.D., 2016b, Giant folds and complex faults in Mesoproterozoic Lemhi subbasin strata of the northern Beaverhead Mountains, Montana and Idaho, in MacLean, J.S., and Sears, J.W., eds., Belt Basin: Window to Mesoproterozoic Earth: Geological Society of America Special Paper 522, 24 p., doi:10.1130/2016.2522(06).

MacKenzie, W.O., 1949, Geology and ore deposits of a section of the Beaverhead Range east of Salm-

on, Idaho: Moscow, University of Idaho, M.S. thesis, 65 p., scale 1:31,000.

Matoush, J.P., 2002, The stratigraphic, sedimentologic, and paleogeographic evolution of the Eocene–Oligocene Grasshopper extensional basin, southwest Montana: Logan, Utah State University, M.S. thesis, 188 p., 4 plates.

McDonald, C., in review, Geologic map of the Argenta 7.5' quadrangle, southwestern Montana: Montana Bureau of Mines and Geology Open-File Report, scale 1:24,000.

McDonald, C., and Lonn, J.D., 2013, Revisions of Mesoproterozoic and Cambrian stratigraphy in the Pioneer and Highland Mountains, southwestern Montana, and resulting implications for the Paleogeography of the Belt Basin: Northwest Geology, v. 42, p. 93–102.

McDonald, C., Elliott, C.G., Vuke, S.M., Lonn, J.D., and Berg, R.B., 2012, Geologic map of the Butte South 30′ x 60′ quadrangle, southwestern Montana: Montana Bureau of Mines and Geology Open-File Report 622, scale 1:100,000.

McDonald, C., and Lonn, J.D. in review, Geologic map of the Ermont 7.5′ quadrangle, southwestern Montana: Montana Bureau of Mines and Geology Open-File Report, scale 1:24,000.

M'Gonigle, J.W., 1994, Geologic map of the Deadman Pass quadrangle, Beaverhead County, southwest Montana: U.S. Geological Survey Geologic Quadrangle Map, GQ-1753, scale 1:24,000.

Mosolf, J.G., in review, Geologic map of the Bannack 7.5′ quadrangle Beaverhead County, Montana: Montana Bureau of Mines and Geology Open-File Report, scale 1:24,000.

Nichols, R., Tabrum, A.R., Barnosky, A.D, and Hill, C.L., 2001, Cenozoic vertebrate paleontology and geology of southwestern Montana and adjacent areas, in Hill, C.L., ed., Mesozoic and Cenozoic paleontology in the Western Plains and Rocky Mountains: Society of Vertebrate Paleontology 61st Annual Meeting Guidebook, p. 79–110.

O'Neill, J.M., Ruppel, E.T., and Lopez, D.A., 2007, Great Divide megashear, Montana, Idaho, and Washington—An intraplate crustal-scale shear zone recurrently active since the Mesoproterozoic: U.S. Geological Survey Open-File Report 2007-1280-A, 10 p.

Pearson, D.M., Anderson, N.D., and Link, P.K., 2017, Zircon U-Pb and Lu-Hf analysis of basement rocks at Bloody Dick Creek and Maiden Peak, southwestern Montana: A record of Paleoproterozoic and Archean plutonism and metamorphism, Northwest Geology, v. 46, p. 29–35.

Pearson, R.C., and Zen, E-an, 1985, Geologic map of the eastern Pioneer Mountains, Beaverhead County, Montana: U.S. Geological Survey Miscellaneous Field Studies Map MF-1806-A, scale 1:50,000.

Roe, W.P., 2010, Tertiary sediments of the Big Hole Valley and Pioneer Mountains, southwestern Montana: Age, provenance, and tectonic implications: Missoula, University of Montana M.S. thesis, 117 p.

Ruppel, E.T., 1975, Precambrian Y sedimentary rocks in east-central Idaho: U.S. Geological Survey Bulletin 889-A, 23 p.

Ruppel, E.T., O'Neill, J.M., and Lopez, D.A., 1993, Geologic map of the Dillon 1° x 2° quadrangle, Idaho and Montana: U.S. Geological Survey Miscellaneous Investigations Series Map I-1803-H, scale 1:250,000.

Sherwin, J.-A., Younggren, E.B, Link, P.K., and Gaschnig, R.M., 2017, Geologic map of the Coyote Creek 7.5' quadrangle, southwest Montana: Montana Bureau of Mines and Geology Geologic Map 67, 1 sheet, scale 1:24,000.

Snee, L.W., 1982, Emplacement and cooling of the Pioneer batholith, southwestern Montana: Columbus, Ohio State University, Ph.D. thesis, 320 p.

Stewart, E.D., Steel, T.D., Stewart, D.E., and Link, P.K., in review, Geologic map of the Gibbonsville, Shewag Lake, and Allan Mountain 7.5' quadrangles, and parts of the Lost Trail Pass and Big Hole Pass 7.5' quadrangles, Lemhi County, Idaho, and Beaverhead County, Montana: Idaho Geological Survey Digital Web Map, scale 1:40,000.

Stroup, C.N., Link, P.K., Jänecke, S.U., Fanning, C.M., Yaxley, G.M., and Beranek, L.P., 2008, Eocene to Oligocene provenance and drainage in extensional basins of southwest Montana and east-central Idaho: Evidence from detrital zircon populations in the Renova Formation and equiva-

lent strata: Arizona Geological Society Digest 22, p. 529–546.

Thomas, R.C., 1995, Tectonic significance of Paleogene sandstone deposits in southwestern Montana: Northwest Geology, v. 24, p. 237–244.

Tietbohl, D., 1986, Middle Proterozoic diamictite beds in the Lemhi Range, east-central Idaho, in Roberts, S.M., ed., Belt Supergroup; A guide to Proterozoic rocks of western Montana and adjacent areas: Montana Bureau of Mines and Geology Special Publication 94, p. 197–207.

Tucker, D.R., 1975, Stratigraphy and structure of Precambrian Y (Belt?) metasedimentary and associated rocks, Goldstone Mountain quadrangle, Lemhi County, Idaho, and Beaverhead County, Montana: Oxford, Ohio, Miami University, Ph.D. dissertation, 221 p., scale 1:48,000.

Tysdal, R.G., 2000, Stratigraphy and depositional environments of Middle Proterozoic rocks, northern part of the Lemhi Range, Lemhi County, Idaho: U.S. Geological Survey Professional Paper 1600, 40 p.

Tysdal, R.G., 2002, Structural geology of the western part of the Lemhi Range, east-central Idaho: U.S. Geological Survey Professional Paper 1659, 33 p.

VanDenburg, C.J., Jänecke, S.U., and McIntosh, W.C., 1998, Three-dimensional strain produced by >50 m.y. of episodic extension, Horse Prairie rift basin, SW Montana, USA: Journal of Structural Geology, v. 20, p. 1747–1767.

Zimbelman, D.R., 1984, Geology of the Polaris 1SE quadrangle, Beaverhead County, Montana: Boulder, University of Colorado, M.S. thesis; 158 p., scale 1:100,000.

APPENDIX A: DATA SHEETS

Table 01NA15. U-Pb geochronologic analyses.

						Isotope Ratios					Apparent Ages (Ma)								
Analysis	U (ppm)	206Pb 204Pb	U/Th	206Pb* 207Pb*	± (%)	207Pb* 235U*	± (%)	206Pb* 238U	± (%)	Error corr.	206Pb* 238U*	± (Ma)	207Pb* 235U	± (Ma)	206Pb* 207Pb*	± (Ma)	Best Age (Ma)	± (Ma)	Conc (%)
-Spot 25	66	46404	1.6	11.0877	1.0	3.0860	3.1	0.2482	3.0	0.95	1429.0	38.0	1429.2	23.9	1429.5	18.8	1429.5	18.8	100.0
-Spot 95	143	56526	1.5	11.0763	0.9	3.0529	3.4	0.2452	3.3	0.96	1413.9	41.7	1421.0	26.2	1431.5	18.1	1431.5	18.1	98.8
-Spot 93	99	303583	0.7	11.0162	0.9	3.2040	3.3	0.2560	3.2	0.96	1469.3	42.4	1458.1	25.9	1441.9	17.0	1441.9	17.0	101.9
-Spot 66	71	424176	2.1	11.0047	0.7	3.0808	4.0	0.2459	3.9	0.98	1417.3	49.4	1427.9	30.3	1443.9	14.0	1443.9	14.0	98.2
-Spot 17	1492	24698	11.5	10.6084	0.9	3.0339	2.8	0.2334	2.6	0.95	1352.4	31.8	1416.2	21.0	1513.4	16.7	1513.4	16.7	89.4
-Spot 67	1809	63304	10.7	10.4620	0.6	3.4589	2.6	0.2625	2.5	0.98	1502.4	33.9	1517.9	20.4	1539.6	10.7	1539.6	10.7	97.6
-Spot 13	56	31275	1.8	10.4182	0.9	3.7881	3.2	0.2862	3.1	0.96	1622.7	44.5	1590.2	25.9	1547.5	16.6	1547.5	16.6	104.9
-Spot 110	61	61971	1.5	9.8753	0.9	3.8876	2.8	0.2784	2.7	0.95	1583.5	37.9	1611.1	22.9	1647.4	16.2	1647.4	16.2	96.1
-Spot 87	81	43320	1.1	9.8326	0.8	4.0182	2.8	0.2865	2.7	0.96	1624.3	38.3	1637.9	22.7	1655.4	15.0	1655.4	15.0	98.1
-Spot 109	156	174620	2.1	9.8048	0.6	4.1354	2.4	0.2941	2.3	0.96	1661.9	33.6	1661.3	19.5	1660.6	12.0	1660.6	12.0	100.1
-Spot 20	59	39740	1.8	9.7776	0.9	4.2893	3.4	0.3042	3.3	0.97	1712.0	50.0	1691.3	28.4	1665.8	16.5	1665.8	16.5	102.8
-Spot 36	239	378191	1.8	9.7259	0.8	4.1688	2.4	0.2941	2.3	0.94	1661.8	33.2	1667.9	19.8	1675.6	15.5	1675.6	15.5	99.2
-Spot 19	78	46992	1.7	9.7172	0.8	4.3443	2.8	0.3062	2.7	0.96	1721.8	40.6	1701.8	23.2	1677.2	15.4	1677.2	15.4	102.7
-Spot 88	74	144622	1.9	9.6972	0.8	4.2419	3.5	0.2983	3.4	0.97	1683.0	49.8	1682.2	28.5	1681.1	15.6	1681.1	15.6	100.1
-Spot 2	85	34191	3.2	9.6643	0.8	4.4351	2.9	0.3109	2.8	0.96	1745.0	42.2	1718.9	23.8	1687.3	14.7	1687.3	14.7	103.4
-Spot 34	113	165315	2.4	9.6510	0.7	4.1401	2.7	0.2898	2.6	0.96	1640.5	38.3	1662.2	22.5	1689.9	13.7	1689.9	13.7	97.1
-Spot 68	114	67710	3.5	9.6443	0.9	4.3112	2.8	0.3016	2.7	0.95	1699.0	39.9	1695.5	23.2	1691.1	16.0	1691.1	16.0	100.5
-Spot 4	207	116410	8.3	9.6324	0.6	4.3702	2.5	0.3053	2.4	0.97	1717.6	36.5	1706.7	20.6	1693.4	11.4	1693.4	11.4	101.4
-Spot 84	183	76147	4.3	9.6288	0.8	4.3947	2.7	0.3069	2.6	0.96	1725.5	39.7	1711.3	22.7	1694.1	14.5	1694.1	14.5	101.9
-Spot 63	62	749856	2.9	9.6195	0.8	4.3257	2.7	0.3018	2.6	0.96	1700.2	38.9	1698.3	22.5	1695.9	14.9	1695.9	14.9	100.3
-Spot 50	123	2373973	4.4	9.5958	1.0	4.2825	3.1	0.2980	3.0	0.95	1681.6	44.1	1690.0	25.9	1700.4	18.6	1700.4	18.6	98.9
-Spot 52	108	251818	5.2	9.5926	0.8	4.3960	2.8	0.3058	2.7	0.96	1720.2	40.2	1711.6	23.0	1701.1	14.3	1701.1	14.3	101.1
-Spot 55	98	198671	2.3	9.5919	0.5	4.4065	2.8	0.3065	2.7	0.98	1723.7	41.2	1713.6	23.0	1701.2	9.7	1701.2	9.7	101.3
-Spot 46	146	241800	1.9	9.5892	0.7	4.5059	2.6	0.3134	2.5	0.96	1757.3	37.9	1732.1	21.3	1701.7	13.1	1701.7	13.1	103.3
-Spot 98	143	94433	1.6	9.5854	0.8	4.2865	2.9	0.2980	2.7	0.96	1681.4	40.6	1690.8	23.6	1702.4	15.6	1702.4	15.6	98.8
-Spot 33	90	50031	3.1	9.5848	0.9	4.4977	3.1	0.3127	2.9	0.96	1753.8	45.2	1730.5	25.5	1702.6	16.1	1702.6	16.1	103.0
-Spot 11	137	109045	4.3	9.5840	0.8	4.5642	2.6	0.3173	2.5	0.95	1776.3	39.1	1742.7	22.0	1702.7	14.6	1702.7	14.6	104.3
-Spot 47	58	2057930	2.0	9.5833	0.6	4.4835	3.0	0.3116	2.9	0.98	1748.7	44.4	1727.9	24.6	1702.8	11.3	1702.8	11.3	102.7
-Spot 59	164	123454	5.0	9.5746	0.9	4.4899	2.6	0.3118	2.5	0.94	1749.5	38.1	1729.1	21.8	1704.5	15.8	1704.5	15.8	102.6
-Spot 5	80	35723	3.0	9.5701	1.0	4.4553	3.0	0.3092	2.8	0.94	1737.0	42.6	1722.7	24.5	1705.4	17.8	1705.4	17.8	101.9
-Spot 94	86	12469	2.4	9.5634	1.2	4.2445	2.9	0.2944	2.7	0.92	1663.5	39.7	1682.7	24.2	1706.7	21.6	1706.7	21.6	97.5
-Spot 44	112	595841	3.8	9.5634	0.9	4.4347	2.8	0.3076	2.7	0.95	1728.8	40.5	1718.8	23.3	1706.7	16.4	1706.7	16.4	101.3
-Spot 108	95	201284	1.8	9.5630	0.7	4.4336	2.8	0.3075	2.7	0.97	1728.4	41.6	1718.6	23.5	1706.7	13.4	1706.7	13.4	101.3
-Spot 16	190	142961	1.3	9.5579	0.7	4.4612	2.5	0.3093	2.4	0.96	1737.0	36.3	1723.8	20.7	1707.7	13.5	1707.7	13.5	101.7
-Spot 54	79	73342	1.8	9.5552	0.7	4.3803	3.3	0.3036	3.2	0.98	1708.9	48.2	1708.6	27.2	1708.2	13.2	1708.2	13.2	100.0
-Spot 92	112	162265	3.7	9.5548	1.0	4.3807	3.1	0.3036	2.9	0.95	1709.0	43.4	1708.7	25.3	1708.3	18.4	1708.3	18.4	100.0
-Spot 79	154	202832	4.8	9.5482	0.9	4.2462	2.9	0.2940	2.7	0.95	1661.7	40.0	1683.0	23.6	1709.6	16.5	1709.6	16.5	97.2
-Spot 10	184	1763615	6.2	9.5473	0.7	4.2684	2.5	0.2956	2.5	0.96	1669.3	36.1	1687.3	20.9	1709.8	12.4	1709.8	12.4	97.6
-Spot 106	97	59917	3.8	9.5462	0.7	4.3809	3.0	0.3033	2.9	0.97	1707.7	43.1	1708.7	24.5	1710.0	13.3	1710.0	13.3	99.9
-Spot 26	110	130300	1.8	9.5454	1.1	4.4130	3.6	0.3055	3.4	0.95	1718.6	51.3	1714.8	29.6	1710.1	20.3	1710.1	20.3	100.5
-Spot 74	87	170430	2.6	9.5451	0.8	4.3543	3.0	0.3014	2.9	0.97	1698.4	43.5	1703.7	24.9	1710.2	14.4	1710.2	14.4	99.3
-Spot 27	482	324620	3.1	9.5447	0.8	4.2989	2.5	0.2976	2.3	0.94	1679.4	34.1	1693.2	20.2	1710.3	15.4	1710.3	15.4	98.2
-Spot 31	123	293982	1.9	9.5425	0.9	4.4186	2.6	0.3058	2.4	0.94	1720.0	36.7	1715.8	21.4	1710.7	16.4	1710.7	16.4	100.5
-Spot 42	263	431798	2.7	9.5410	0.8	4.3096	2.7	0.2982	2.6	0.96	1682.5	38.9	1695.2	22.5	1711.0	14.0	1711.0	14.0	98.3
-Spot 70	299	245177	4.9	9.5378	0.9	4.2324	2.8	0.2928	2.6	0.94	1655.4	38.1	1680.3	22.7	1711.6	16.8	1711.6	16.8	96.7
-Spot 21	138	99404	3.8	9.5365	1.0	4.3550	3.0	0.3012	2.8	0.94	1697.3	41.6	1703.8	24.6	1711.8	19.2	1711.8	19.2	99.2
-Spot 96	153	755272	4.2	9.5360	0.7	4.2735	2.4	0.2956	2.3	0.96	1669.3	34.4	1688.3	20.1	1711.9	12.8	1711.9	12.8	97.5
-Spot 9	317	201062	1.0	9.5269	0.9	4.3638	2.7	0.3015	2.5	0.94	1698.8	37.3	1705.5	22.0	1713.7	17.3	1713.7	17.3	99.1
-Spot 30	155	121172	2.7	9.5235	0.7	4.3335	2.3	0.2993	2.2	0.95	1687.9	33.2	1699.8	19.4	1714.4	13.4	1714.4	13.4	98.5
-Spot 102	165	225744	3.0	9.5220	0.7	4.4055	2.7	0.3042	2.6	0.96	1712.3	38.9	1713.4	22.3	1714.6	13.7	1714.6	13.7	99.9
-Spot 78	199	98908	6.5	9.5218	0.7	4.4230	2.7	0.3054	2.6	0.97	1718.3	38.9	1716.7	22.1	1714.7	12.5	1714.7	12.5	100.2
-Spot 40	64	31832	13.4	9.5142	0.7	4.3912	2.9	0.3030	2.8	0.97	1706.2	42.6	1710.7	24.2	1716.1	13.3	1716.1	13.3	99.4
-Spot 1	190	155997	3.2	9.5091	0.8	4.2638	2.7	0.2941	2.5	0.95	1661.8	37.1	1686.4	21.8	1717.1	14.5	1717.1	14.5	96.8
-Spot 24	401	792592	3.4	9.5067	0.8	4.3224	2.2	0.2980	2.1	0.94	1681.5	30.6	1697.6	18.2	1717.6	13.9	1717.6	13.9	97.9
-Spot 49	119	60863	2.3	9.5052	0.6	4.3788	2.5	0.3019	2.5	0.97	1700.6	36.7	1708.4	20.9	1717.9	11.0	1717.9	11.0	99.0
-Spot 3	82	37537	1.4	9.4978	0.7	4.5432	3.0	0.3130	2.9	0.97	1755.2	45.2	1738.9	25.2	1719.3	13.5	1719.3	13.5	102.1
-Spot 53	98	52538	2.6	9.4954	0.8	4.4785	2.7	0.3084	2.6	0.96	1733.0	40.0	1727.0	22.8	1719.8	14.3	1719.8	14.3	100.8
-Spot 45	62	131433	3.1	9.4909	0.7	4.4304	3.3	0.3050	3.3	0.98	1715.9	49.1	1718.0	27.6	1720.7	12.4	1720.7	12.4	99.7
-Spot 77	199	206031	3.7	9.4875	0.9	4.3480	2.8	0.2992	2.6	0.94	1687.3	39.2	1702.5	23.1	1721.3	17.2	1721.3	17.2	98.0
-Spot 43	89	73016	2.8	9.4858	0.9	4.4694	3.2	0.3075	3.1	0.96	1728.3	46.9	1725.3	26.8	1721.6	17.0	1721.6	17.0	100.4
-Spot 18	189	109746	3.0	9.4837	0.8	4.2492	2.8	0.2923	2.6	0.95	1652.8	38.2	1683.6	22.6	1722.1	15.6	1722.1	15.6	96.0

						Isotope Ratios					Apparent Ages (Ma)								
Analysis	U (ppm)	206Pb 204Pb	U/Th	206Pb* 207Pb*	± (%)	207Pb* 235U*	± (%)	206Pb* 238U	± (%)	Error corr.	206Pb* 238U*	± (Ma)	207Pb* 235U	± (Ma)	206Pb* 207Pb*	± (Ma)	Best Age (Ma)	± (Ma)	Conc (%)
-Spot 60	91	789573	2.4	9.4741	0.7	4.5146	2.4	0.3102	2.3	0.96	1741.7	35.7	1733.7	20.3	1723.9	13.3	1723.9	13.3	101.0
-Spot 107	79	69793	1.4	9.4690	0.9	4.3916	3.5	0.3016	3.4	0.96	1699.2	50.9	1710.8	29.2	1724.9	17.0	1724.9	17.0	98.5
-Spot 41	83	39094	1.8	9.4648	1.0	4.4997	3.2	0.3089	3.0	0.94	1735.2	46.0	1730.9	26.6	1725.7	19.3	1725.7	19.3	100.6
-Spot 61	60	26094	4.7	9.4625	0.8	4.5515	2.8	0.3124	2.7	0.96	1752.3	41.5	1740.4	23.5	1726.2	14.8	1726.2	14.8	101.5
-Spot 89	148	134796	3.4	9.4602	0.8	4.4123	2.7	0.3027	2.6	0.96	1704.9	38.5	1714.6	22.2	1726.6	14.1	1726.6	14.1	98.7
-Spot 12	101	33131	2.7	9.4531	0.6	4.5967	2.6	0.3151	2.5	0.97	1766.0	38.8	1748.7	21.6	1728.0	11.4	1728.0	11.4	102.2
-Spot 75	67	106845	2.3	9.4531	0.9	4.5005	3.1	0.3086	2.9	0.95	1733.6	44.4	1731.1	25.5	1728.0	17.1	1728.0	17.1	100.3
-Spot 99	147	49837	3.8	9.4449	0.9	4.1438	3.0	0.2839	2.9	0.95	1610.8	41.0	1663.0	24.7	1729.6	17.2	1729.6	17.2	93.1
-Spot 82	53	335432	1.3	9.4380	0.9	4.5231	2.9	0.3096	2.8	0.95	1738.8	42.3	1735.2	24.4	1730.9	17.4	1730.9	17.4	100.5
-Spot 38	183	129266	2.1	9.4374	0.9	4.4826	2.4	0.3068	2.3	0.93	1725.0	34.1	1727.8	20.2	1731.0	16.9	1731.0	16.9	99.7
-Spot 97	92	67048	3.6	9.4339	0.8	4.4747	3.3	0.3062	3.2	0.97	1721.8	47.9	1726.3	27.1	1731.7	14.1	1731.7	14.1	99.4
-Spot 15	270	180140	3.2	9.4288	0.9	4.4665	2.8	0.3054	2.7	0.95	1718.2	40.1	1724.8	23.2	1732.7	15.6	1732.7	15.6	99.2
-Spot 23	45	40577	1.5	9.4104	0.8	4.6949	3.6	0.3204	3.5	0.98	1791.8	55.4	1766.3	30.4	1736.3	14.4	1736.3	14.4	103.2
-Spot 85	102	48845	2.0	9.4067	0.8	4.3913	2.6	0.2996	2.5	0.95	1689.3	37.5	1710.7	21.9	1737.0	14.6	1737.0	14.6	97.3
-Spot 103	94	98599	1.9	9.4003	0.7	4.4408	2.4	0.3028	2.3	0.96	1705.0	34.2	1720.0	19.7	1738.3	12.0	1738.3	12.0	98.1
-Spot 7	124	103413	2.3	9.3882	0.8	4.6201	2.9	0.3146	2.8	0.96	1763.2	42.9	1752.9	24.1	1740.6	14.2	1740.6	14.2	101.3
-Spot 28	36	20703	3.7	9.3864	0.9	4.7414	2.7	0.3228	2.5	0.94	1803.3	40.1	1774.6	22.7	1741.0	16.7	1741.0	16.7	103.6
-Spot 37	59	25188	10.4	9.3826	1.0	4.4857	3.4	0.3052	3.3	0.96	1717.3	49.6	1728.3	28.5	1741.7	17.7	1741.7	17.7	98.6
-Spot 90	166	78757	1.2	9.3771	0.9	4.5255	2.8	0.3078	2.7	0.95	1729.7	40.8	1735.7	23.5	1742.8	15.8	1742.8	15.8	99.3
-Spot 83	41	186493	5.2	9.3706	0.8	4.6178	3.3	0.3138	3.2	0.97	1759.5	49.6	1752.5	27.6	1744.1	13.8	1744.1	13.8	100.9
-Spot 80	78	35476	1.8	9.3704	0.7	4.7358	2.7	0.3218	2.6	0.96	1798.7	41.4	1773.6	23.0	1744.1	13.5	1744.1	13.5	103.1
-Spot 76	34	29762	2.7	9.3660	0.9	4.4724	3.3	0.3038	3.2	0.97	1710.1	47.8	1725.9	27.4	1745.0	15.8	1745.0	15.8	98.0
-Spot 73	108	159340	4.0	9.3601	0.6	4.4582	2.8	0.3026	2.7	0.98	1704.4	41.0	1723.2	23.2	1746.1	11.1	1746.1	11.1	97.6
-Spot 58	243	127385	1.2	9.3487	0.8	4.4644	2.6	0.3027	2.4	0.96	1704.7	36.5	1724.4	21.2	1748.3	13.8	1748.3	13.8	97.5
-Spot 101	109	102585	4.0	9.3209	0.8	4.6112	2.8	0.3117	2.7	0.96	1749.2	41.1	1751.3	23.3	1753.8	14.4	1753.8	14.4	99.7
-Spot 35	56	269459	3.0	9.3002	0.7	4.7992	3.1	0.3237	3.0	0.97	1807.8	47.2	1784.8	25.9	1757.9	13.1	1757.9	13.1	102.8
-Spot 29	141	129695	3.9	9.2972	0.8	4.4179	3.0	0.2979	2.8	0.96	1680.9	42.1	1715.7	24.6	1758.5	15.2	1758.5	15.2	95.6
-Spot 100	88	20988	6.3	9.2831	0.8	4.7298	3.4	0.3184	3.3	0.97	1782.1	51.6	1772.5	28.5	1761.2	14.2	1761.2	14.2	101.2
-Spot 57	194	92763	3.7	9.2631	0.7	4.6383	2.9	0.3116	2.8	0.97	1748.7	42.3	1756.2	23.8	1765.2	12.8	1765.2	12.8	99.1
-Spot 105	182	217573	5.9	9.2374	0.6	4.6942	2.6	0.3145	2.6	0.97	1762.8	39.8	1766.2	22.2	1770.2	10.9	1770.2	10.9	99.6
-Spot 8	204	321096	1.9	9.2368	0.7	4.6431	2.9	0.3110	2.8	0.97	1745.9	42.7	1757.0	24.1	1770.4	12.9	1770.4	12.9	98.6
-Spot 91	71	30210	3.3	9.1991	1.1	4.7662	2.9	0.3180	2.7	0.93	1779.9	41.9	1779.0	24.3	1777.8	19.4	1777.8	19.4	100.1
-Spot 81	90	95949	1.8	9.1984	0.8	4.7565	2.8	0.3173	2.7	0.96	1776.6	42.2	1777.3	23.7	1778.0	14.3	1778.0	14.3	99.9
-Spot 62	140	182714	4.3	9.1801	0.9	4.8373	3.1	0.3221	2.9	0.96	1799.8	46.1	1791.4	25.7	1781.6	15.6	1781.6	15.6	101.0
-Spot 22	215	115359	3.2	9.1735	0.9	4.7904	2.8	0.3187	2.7	0.95	1783.5	41.7	1783.2	23.7	1782.9	15.9	1782.9	15.9	100.0
-Spot 71	43	77377	1.6	9.1590	1.1	4.8523	4.2	0.3223	4.1	0.97	1801.1	64.3	1794.0	35.6	1785.8	19.4	1785.8	19.4	100.9
-Spot 69	86	37860	3.7	9.1054	0.7	4.5844	2.9	0.3027	2.8	0.97	1704.9	42.6	1746.4	24.5	1796.5	13.4	1796.5	13.4	94.9
-Spot 48	88	49204	2.7	9.0963	0.8	5.0394	2.5	0.3325	2.3	0.95	1850.3	37.8	1826.0	21.0	1798.3	14.4	1798.3	14.4	102.9
-Spot 32	130	116391	1.6	8.9930	0.9	5.1083	2.7	0.3332	2.5	0.94	1853.8	40.1	1837.5	22.5	1819.1	16.9	1819.1	16.9	101.9
-Spot 86	53	102525	1.7	8.9215	0.9	5.0681	3.8	0.3279	3.7	0.97	1828.4	58.9	1830.8	32.3	1833.5	16.4	1833.5	16.4	99.7
-Spot 64	205	176257	3.0	8.7834	0.8	5.1882	2.2	0.3305	2.0	0.94	1840.8	32.7	1850.7	18.6	1861.8	13.8	1861.8	13.8	98.9
-Spot 56	36	27713	1.1	6.8430	1.0	8.5762	3.1	0.4256	2.9	0.95	2286.0	56.6	2294.0	28.2	2301.2	16.6	2301.2	16.6	99.3
-Spot 104	217	1244771	4.1	6.4668	0.7	9.4980	2.5	0.4455	2.4	0.96	2375.1	47.5	2387.4	22.9	2397.8	11.9	2397.8	11.9	99.1
-Spot 65	82	73093	3.0	6.2344	0.8	10.2167	2.5	0.4620	2.4	0.95	2448.2	49.2	2454.6	23.4	2459.9	12.9	2459.9	12.9	99.5
-Spot 72	36	44601	1.7	4.1663	0.7	20.9111	3.2	0.6319	3.1	0.97	3157.0	77.6	3134.5	31.0	3120.1	11.9	3120.1	11.9	101.2

Table 02NA15. U-Pb geochronologic analyses.

						Isotope Ratios					Apparent Ages (Ma)								
Analysis	U (ppm)	206Pb 204Pb	U/Th	206Pb* 207Pb*	± (%)	207Pb* 235U*	± (%)	206Pb* 238U	± (%)	Error corr.	206Pb* 238U*	± (Ma)	207Pb* 235U	± (Ma)	206Pb* 207Pb*	± (Ma)	Best Age (Ma)	± (Ma)	Conc (%)
-Spot 77	177	44068	2.4	11.1294	0.6	3.0046	1.7	0.2425	1.6	0.94	1399.8	20.4	1408.8	13.1	1422.4	10.8	1422.4	10.8	98.4
-Spot 69	123	30335	1.5	11.1242	0.7	3.1225	2.2	0.2519	2.1	0.95	1448.4	26.6	1438.3	16.6	1423.3	12.4	1423.3	12.4	101.8
-Spot 78	168	56909	2.4	11.1205	0.6	3.1188	2.1	0.2515	2.0	0.96	1446.4	25.5	1437.3	15.8	1423.9	11.5	1423.9	11.5	101.6
-Spot 22	101	192563	0.9	11.1007	0.6	3.1377	3.1	0.2526	3.0	0.98	1452.0	39.1	1442.0	23.7	1427.3	12.4	1427.3	12.4	101.7
-Spot 83	33	117423	0.9	11.0877	1.1	3.1870	4.2	0.2563	4.1	0.97	1470.8	54.0	1454.0	32.8	1429.5	20.6	1429.5	20.6	102.9
-Spot 75	284	452301	1.7	11.0071	0.4	3.1277	2.0	0.2497	1.9	0.97	1436.9	24.9	1439.5	15.3	1443.5	8.4	1443.5	8.4	99.5
-Spot 13	168	126192	0.7	10.9262	0.6	3.0866	2.1	0.2446	2.0	0.96	1410.5	25.5	1429.4	16.0	1457.5	10.7	1457.5	10.7	96.8
-Spot 59	315	335703	0.8	10.9022	0.5	3.1336	2.0	0.2478	1.9	0.96	1427.0	24.5	1441.0	15.3	1461.7	9.9	1461.7	9.9	97.6
-Spot 104	134	99764	1.0	10.7555	0.6	3.2380	1.9	0.2526	1.8	0.94	1451.8	23.4	1466.3	14.8	1487.4	12.3	1487.4	12.3	97.6
-Spot 106	117	48960	2.5	10.2015	0.7	3.8854	2.6	0.2875	2.5	0.97	1628.9	36.5	1610.6	21.1	1586.9	12.2	1586.9	12.2	102.6
-Spot 5	1628	487809	35.8	10.1874	0.5	3.9057	1.5	0.2886	1.4	0.94	1634.4	19.8	1614.9	11.8	1589.5	8.9	1589.5	8.9	102.8
-Spot 91	576	97418	1.6	10.0523	0.5	3.6224	1.6	0.2641	1.5	0.94	1510.8	20.0	1554.5	12.5	1614.4	9.6	1614.4	9.6	93.6
-Spot 21	1688	302030	16.0	9.9284	0.6	4.1580	1.4	0.2994	1.3	0.89	1688.4	18.7	1665.8	11.5	1637.4	11.8	1637.4	11.8	103.1
-Spot 38	150	48945	2.3	9.8067	0.6	4.0582	2.1	0.2886	2.0	0.96	1634.7	28.9	1646.0	16.9	1660.3	10.6	1660.3	10.6	98.5
-Spot 98	313	88867	2.1	9.7706	0.7	4.1446	2.0	0.2937	1.8	0.93	1660.0	26.8	1663.1	16.2	1667.1	13.8	1667.1	13.8	99.6
-Spot 71	262	164595	2.1	9.7127	0.5	4.3263	2.1	0.3048	2.0	0.97	1714.9	30.2	1698.4	17.0	1678.1	9.3	1678.1	9.3	102.2
-Spot 110	300	43909	3.6	9.7100	0.5	4.3637	1.6	0.3073	1.5	0.94	1727.4	22.5	1705.5	13.0	1678.6	9.7	1678.6	9.7	102.9
-Spot 96	36	55200	0.8	9.7025	0.8	4.2971	4.1	0.3024	4.0	0.98	1703.1	59.9	1692.8	33.7	1680.0	15.4	1680.0	15.4	101.4
-Spot 29	78	13706	1.2	9.6919	0.5	4.2791	3.1	0.3008	3.1	0.98	1695.2	45.7	1689.4	25.6	1682.1	10.0	1682.1	10.0	100.8
-Spot 61	1325	942963	4.5	9.6819	0.5	4.1094	1.3	0.2886	1.2	0.93	1634.3	17.6	1656.2	10.7	1684.0	9.0	1684.0	9.0	97.1
-Spot 44	1900	284704	4.9	9.6443	0.5	4.1292	1.4	0.2888	1.3	0.93	1635.6	19.0	1660.1	11.5	1691.2	9.6	1691.2	9.6	96.7
-Spot 103	207	99145	1.4	9.6284	0.6	4.2715	2.0	0.2983	1.9	0.96	1682.8	28.0	1687.9	16.3	1694.2	10.8	1694.2	10.8	99.3
-Spot 76	123	19839	2.0	9.6280	0.7	4.3549	2.6	0.3041	2.5	0.97	1711.6	37.4	1703.8	21.3	1694.3	12.4	1694.3	12.4	101.0
-Spot 97	283	50653	3.3	9.6179	0.4	4.3579	1.8	0.3040	1.7	0.97	1711.1	25.8	1704.4	14.6	1696.2	7.7	1696.2	7.7	100.9
-Spot 74	222	96977	1.8	9.6175	0.4	4.4305	2.0	0.3090	1.9	0.98	1736.0	29.6	1718.1	16.5	1696.3	8.1	1696.3	8.1	102.3
-Spot 85	164	45264	2.5	9.6159	0.6	4.3223	2.1	0.3014	2.0	0.96	1698.5	30.3	1697.6	17.4	1696.6	10.9	1696.6	10.9	100.1
-Spot 8	205	36369	5.7	9.6159	0.5	4.2907	1.5	0.2992	1.4	0.95	1687.5	20.9	1691.6	12.2	1696.6	8.6	1696.6	8.6	99.5
-Spot 101	178	162390	1.9	9.6157	0.5	4.3060	2.0	0.3003	1.9	0.96	1692.8	28.0	1694.5	16.1	1696.6	10.1	1696.6	10.1	99.8
-Spot 64	97	210650	1.2	9.6081	0.5	4.3756	2.3	0.3049	2.2	0.97	1715.6	33.3	1707.7	18.8	1698.1	9.9	1698.1	9.9	101.0
-Spot 49	226	89472	2.2	9.6048	0.5	4.3439	2.2	0.3026	2.1	0.97	1704.2	32.1	1701.7	18.2	1698.7	9.8	1698.7	9.8	100.3
-Spot 89	241	174195	1.0	9.6011	0.6	4.2210	1.8	0.2939	1.7	0.95	1661.1	25.1	1678.1	14.8	1699.4	10.3	1699.4	10.3	97.7
-Spot 100	136	52415	1.8	9.5981	0.5	4.5025	2.3	0.3134	2.3	0.98	1757.5	35.0	1731.4	19.3	1700.0	8.8	1700.0	8.8	103.4
-Spot 4	210	68624	2.2	9.5860	0.4	4.2921	2.0	0.2984	2.0	0.98	1683.4	29.1	1691.8	16.6	1702.3	8.1	1702.3	8.1	98.9
-Spot 30	265	46812	1.6	9.5856	0.6	4.4186	2.3	0.3072	2.2	0.97	1726.8	33.2	1715.8	18.8	1702.4	10.7	1702.4	10.7	101.4
-Spot 42	1308	346979	7.1	9.5851	0.6	4.2959	1.7	0.2986	1.6	0.93	1684.6	23.6	1692.6	14.0	1702.5	11.3	1702.5	11.3	98.9
-Spot 65	416	471270	2.6	9.5843	0.5	4.2212	1.5	0.2934	1.4	0.94	1658.6	20.5	1678.2	12.3	1702.7	9.3	1702.7	9.3	97.4
-Spot 108	127	44434	1.7	9.5794	0.6	4.4198	2.3	0.3071	2.3	0.97	1726.3	34.3	1716.1	19.4	1703.6	10.9	1703.6	10.9	101.3
-Spot 1	563	123058	0.9	9.5725	0.4	4.1960	1.4	0.2913	1.3	0.95	1648.1	19.2	1673.2	11.4	1704.9	7.7	1704.9	7.7	96.7
-Spot 99	245	62442	8.8	9.5715	0.5	4.3504	1.6	0.3020	1.5	0.95	1701.2	22.3	1703.0	12.9	1705.1	9.0	1705.1	9.0	99.8
-Spot 48	274	132293	3.8	9.5672	0.5	4.3100	1.9	0.2991	1.9	0.97	1686.6	28.1	1695.3	16.1	1705.9	8.5	1705.9	8.5	98.9
-Spot 68	264	96512	1.7	9.5655	0.6	4.3748	1.9	0.3035	1.8	0.95	1708.7	27.1	1707.6	15.8	1706.3	11.5	1706.3	11.5	100.1
-Spot 54	151	1084314	0.9	9.5638	0.5	4.3801	2.0	0.3038	2.0	0.96	1710.2	29.3	1708.6	16.7	1706.6	10.0	1706.6	10.0	100.2
-Spot 35	254	116694	2.4	9.5623	0.6	4.3088	1.7	0.2988	1.6	0.94	1685.5	23.7	1695.0	14.1	1706.9	11.1	1706.9	11.1	98.7
-Spot 40	229	88133	2.6	9.5532	0.5	4.3998	2.2	0.3048	2.1	0.97	1715.3	32.1	1712.3	18.1	1708.6	9.1	1708.6	9.1	100.4
-Spot 41	99	31878	2.9	9.5454	0.5	4.3500	2.4	0.3011	2.4	0.98	1697.0	35.7	1702.9	20.2	1710.1	9.7	1710.1	9.7	99.2
-Spot 79	210	65349	1.0	9.5362	0.4	4.3617	2.2	0.3017	2.2	0.98	1699.6	32.7	1705.1	18.4	1711.9	8.2	1711.9	8.2	99.3
-Spot 28	336	120994	2.3	9.5271	0.5	4.3317	1.6	0.2993	1.6	0.95	1687.9	23.0	1699.4	13.5	1713.7	9.4	1713.7	9.4	98.5
-Spot 17	597	5964076	2.5	9.5250	0.5	4.3005	1.5	0.2971	1.4	0.95	1676.8	21.3	1693.5	12.5	1714.1	8.5	1714.1	8.5	97.8
-Spot 87	57	10356	1.9	9.5219	0.8	4.5195	2.2	0.3121	2.0	0.93	1751.1	30.9	1734.6	18.0	1714.7	14.7	1714.7	14.7	102.1
-Spot 3	148	71246	2.4	9.5119	0.6	4.3276	2.5	0.2985	2.5	0.97	1684.1	36.4	1698.6	21.0	1716.6	11.9	1716.6	11.9	98.1
-Spot 70	473	791868	1.5	9.5081	0.6	4.4064	1.7	0.3039	1.6	0.93	1710.4	24.4	1713.5	14.4	1717.3	11.4	1717.3	11.4	99.6
-Spot 60	418	129398	1.5	9.5076	0.5	4.2698	1.8	0.2944	1.8	0.97	1663.6	26.2	1687.6	15.2	1717.4	8.5	1717.4	8.5	96.9
-Spot 39	384	87089	2.3	9.5019	0.6	4.4383	2.0	0.3059	1.9	0.95	1720.3	28.8	1719.5	16.5	1718.5	11.0	1718.5	11.0	100.1
-Spot 81	93	34565	2.0	9.4968	0.5	4.3808	2.8	0.3017	2.8	0.98	1699.9	41.4	1708.7	23.3	1719.5	9.2	1719.5	9.2	98.9
-Spot 88	671	53895	1.5	9.4954	0.5	4.0272	1.9	0.2773	1.8	0.96	1577.9	24.9	1639.7	15.1	1719.8	9.3	1719.8	9.3	91.8
-Spot 80	455	195647	0.8	9.4930	0.4	4.2812	1.6	0.2948	1.6	0.98	1665.3	23.6	1689.7	13.6	1720.3	6.6	1720.3	6.6	96.8
-Spot 25	373	149978	1.8	9.4928	0.6	4.3347	1.7	0.2984	1.6	0.94	1683.5	23.9	1700.0	14.2	1720.3	10.9	1720.3	10.9	97.9

						Isotope Ratios					Apparent Ages (Ma)								
Analysis	U (ppm)	206Pb 204Pb	U/Th	206Pb* 207Pb*	± (%)	207Pb* 235U*	± (%)	206Pb* 238U	± (%)	Error corr.	206Pb* 238U*	± (Ma)	207Pb* 235U	± (Ma)	206Pb* 207Pb*	± (Ma)	Best Age (Ma)	± (Ma)	Conc (%)
-Spot 82	280	53532	2.3	9.4897	0.5	4.3802	1.6	0.3015	1.5	0.95	1698.6	22.1	1708.6	13.0	1720.9	9.4	1720.9	9.4	98.7
-Spot 16	145	536357	1.9	9.4894	0.6	4.4204	2.3	0.3042	2.2	0.97	1712.3	33.8	1716.2	19.2	1720.9	10.4	1720.9	10.4	99.5
-Spot 43	288	63115	1.9	9.4883	0.7	4.4485	2.0	0.3061	1.9	0.95	1721.6	29.0	1721.4	16.8	1721.2	12.0	1721.2	12.0	100.0
-Spot 7	478	255907	6.2	9.4865	0.5	4.2663	1.5	0.2935	1.4	0.94	1659.2	20.2	1686.9	12.1	1721.5	9.6	1721.5	9.6	96.4
-Spot 72	195	379902	1.7	9.4758	0.6	4.4035	2.3	0.3026	2.3	0.96	1704.3	33.8	1713.0	19.4	1723.6	11.8	1723.6	11.8	98.9
-Spot 24	245	77841	2.1	9.4743	0.6	4.3993	1.6	0.3023	1.5	0.93	1702.7	22.6	1712.2	13.4	1723.9	10.6	1723.9	10.6	98.8
-Spot 11	113	41621	2.1	9.4739	0.5	4.4327	2.3	0.3046	2.3	0.97	1714.0	34.3	1718.5	19.4	1724.0	9.9	1724.0	9.9	99.4
-Spot 53	131	70762	1.4	9.4730	0.5	4.4378	1.9	0.3049	1.9	0.97	1715.6	28.2	1719.4	16.1	1724.1	9.1	1724.1	9.1	99.5
-Spot 34	169	219823	2.5	9.4612	0.7	4.3476	1.9	0.2983	1.7	0.92	1683.0	25.5	1702.4	15.5	1726.4	13.6	1726.4	13.6	97.5
-Spot 23	249	102633	1.6	9.4582	0.7	4.5202	1.8	0.3101	1.7	0.93	1741.1	25.4	1734.7	14.9	1727.0	12.2	1727.0	12.2	100.8
-Spot 94	95	74327	1.0	9.4512	0.6	4.5315	2.1	0.3106	2.0	0.96	1743.8	30.5	1736.8	17.3	1728.4	10.5	1728.4	10.5	100.9
-Spot 92	219	60395	1.7	9.4498	0.5	4.3945	1.8	0.3012	1.7	0.96	1697.2	25.5	1711.3	14.7	1728.6	8.6	1728.6	8.6	98.2
-Spot 9	636	8218645	6.4	9.4454	0.6	4.3032	1.6	0.2948	1.5	0.93	1665.4	22.1	1694.0	13.3	1729.5	10.7	1729.5	10.7	96.3
-Spot 56	286	658873	2.4	9.4451	0.5	4.4423	1.4	0.3043	1.3	0.94	1712.6	20.1	1720.3	11.8	1729.5	9.0	1729.5	9.0	99.0
-Spot 6	99	115256	18.4	9.4407	0.5	4.4910	2.4	0.3075	2.4	0.98	1728.4	36.3	1729.3	20.3	1730.4	8.6	1730.4	8.6	99.9
-Spot 50	182	152811	1.9	9.4358	0.6	4.5040	2.0	0.3082	1.9	0.95	1732.0	28.7	1731.7	16.4	1731.4	10.8	1731.4	10.8	100.0
-Spot 84	381	358069	1.9	9.4287	0.5	4.4855	1.8	0.3067	1.7	0.96	1724.6	25.7	1728.3	14.7	1732.7	9.4	1732.7	9.4	99.5
-Spot 105	245	256341	1.7	9.4284	0.6	4.4829	1.8	0.3065	1.6	0.93	1723.7	24.9	1727.8	14.6	1732.8	11.7	1732.8	11.7	99.5
-Spot 10	178	13436212	1.0	9.4152	0.5	4.5046	2.5	0.3076	2.4	0.98	1728.9	37.0	1731.8	20.7	1735.4	9.2	1735.4	9.2	99.6
-Spot 62	710	529998	5.0	9.4081	0.4	4.4098	1.3	0.3009	1.2	0.95	1695.8	17.9	1714.2	10.5	1736.7	7.4	1736.7	7.4	97.6
-Spot 15	904	139030	2.8	9.4039	0.5	4.3762	1.5	0.2985	1.4	0.94	1683.7	21.4	1707.9	12.6	1737.6	9.3	1737.6	9.3	96.9
-Spot 37	184	135356	3.1	9.3850	0.4	4.5733	1.9	0.3113	1.9	0.98	1747.1	29.0	1744.4	16.2	1741.2	7.8	1741.2	7.8	100.3
-Spot 95	441	201447	2.0	9.3737	0.6	4.6276	1.7	0.3146	1.5	0.93	1763.3	23.7	1754.3	13.8	1743.5	11.2	1743.5	11.2	101.1
-Spot 12	140	36610	1.7	9.3561	0.5	4.4599	2.1	0.3026	2.0	0.97	1704.4	30.1	1723.6	17.3	1746.9	9.9	1746.9	9.9	97.6
-Spot 51	310	279920	1.4	9.3526	0.5	4.4432	1.7	0.3014	1.6	0.95	1698.2	23.7	1720.4	13.9	1747.6	9.5	1747.6	9.5	97.2
-Spot 36	807	316530	2.1	9.3489	0.5	4.3988	1.6	0.2983	1.5	0.95	1682.6	22.4	1712.1	13.1	1748.3	9.0	1748.3	9.0	96.2
-Spot 45	170	924178	1.3	9.3456	0.6	4.4123	2.1	0.2991	2.0	0.96	1686.7	29.4	1714.7	17.1	1749.0	10.4	1749.0	10.4	96.4
-Spot 66	176	226206	4.1	9.3351	0.6	4.6965	2.2	0.3180	2.2	0.97	1779.8	33.5	1766.6	18.7	1751.0	10.5	1751.0	10.5	101.6
-Spot 26	348	89672	2.3	9.3176	0.6	4.5029	1.5	0.3043	1.3	0.91	1712.6	20.0	1731.5	12.2	1754.4	11.3	1754.4	11.3	97.6
-Spot 47	337	177856	1.7	9.3159	0.5	4.6917	1.7	0.3170	1.7	0.95	1775.0	25.8	1765.8	14.6	1754.8	9.6	1754.8	9.6	101.2
-Spot 52	196	74515	3.5	9.3101	0.5	4.6553	1.9	0.3143	1.8	0.96	1762.0	28.1	1759.2	15.9	1755.9	9.8	1755.9	9.8	100.3
-Spot 57	134	894623	0.8	9.2965	0.5	4.7476	2.4	0.3201	2.3	0.97	1790.2	36.2	1775.7	19.9	1758.6	9.9	1758.6	9.9	101.8
-Spot 102	362	169091	1.9	9.2905	0.5	4.5920	1.4	0.3094	1.3	0.93	1737.8	19.7	1747.8	11.6	1759.8	9.3	1759.8	9.3	98.8
-Spot 18	625	263926	2.0	9.2817	0.5	4.7562	1.4	0.3202	1.3	0.93	1790.6	20.8	1777.2	12.0	1761.5	9.6	1761.5	9.6	101.6
-Spot 107	84	25138	3.9	9.2505	0.5	4.8583	3.0	0.3259	3.0	0.99	1818.7	47.0	1795.0	25.4	1767.7	9.2	1767.7	9.2	102.9
-Spot 31	641	2072976	9.7	9.2500	0.6	4.6983	1.5	0.3152	1.4	0.93	1766.2	21.3	1766.9	12.4	1767.8	10.1	1767.8	10.1	99.9
-Spot 86	225	220146	2.5	9.2370	0.7	4.6827	2.1	0.3137	2.0	0.95	1758.9	31.2	1764.1	17.8	1770.3	12.1	1770.3	12.1	99.4
-Spot 93	85	87024	3.9	9.1819	0.6	4.7956	2.8	0.3194	2.8	0.98	1786.6	43.4	1784.1	23.9	1781.2	10.3	1781.2	10.3	100.3
-Spot 19	93	38169	1.4	9.1701	1.1	4.6072	2.4	0.3064	2.1	0.90	1723.0	32.4	1750.6	19.9	1783.6	19.3	1783.6	19.3	96.6
-Spot 14	506	30748398	2.2	9.1404	0.5	4.7461	1.7	0.3146	1.7	0.96	1763.4	25.7	1775.4	14.5	1789.5	8.7	1789.5	8.7	98.5
-Spot 46	124	159136	3.2	9.1346	0.6	4.8728	1.9	0.3228	1.8	0.96	1803.5	28.8	1797.6	16.1	1790.7	10.2	1790.7	10.2	100.7
-Spot 27	423	497684	1.9	9.1293	0.4	4.6882	1.5	0.3104	1.4	0.95	1742.8	21.3	1765.1	12.3	1791.7	8.1	1791.7	8.1	97.3
-Spot 33	457	335797	3.1	9.0549	0.5	4.9892	1.6	0.3277	1.5	0.95	1827.0	24.0	1817.5	13.5	1806.6	9.4	1806.6	9.4	101.1
-Spot 67	180	49306	1.7	8.9444	0.5	5.2053	1.9	0.3377	1.8	0.97	1875.5	29.4	1853.5	15.9	1828.9	8.5	1828.9	8.5	102.5
-Spot 109	261	162209	0.8	8.8901	0.5	5.2053	1.8	0.3356	1.8	0.97	1865.6	28.8	1853.5	15.6	1839.9	8.4	1839.9	8.4	101.4
-Spot 90	430	119897	2.2	8.8085	0.4	5.2677	1.4	0.3365	1.4	0.96	1869.9	22.3	1863.6	12.1	1856.6	6.8	1856.6	6.8	100.7
-Spot 58	146	76642	2.1	6.5129	0.5	9.6330	2.1	0.4550	2.0	0.97	2417.6	41.0	2400.3	19.3	2385.7	8.6	2385.7	8.6	101.3
-Spot 20	188	1180381	3.5	5.8460	0.5	11.1308	2.1	0.4719	2.1	0.97	2492.1	42.4	2534.1	19.8	2568.0	9.0	2568.0	9.0	97.0
-Spot 32	272	3176075	1.9	5.7600	0.5	11.5770	1.7	0.4836	1.6	0.96	2543.1	34.4	2570.8	16.0	2592.8	8.0	2592.8	8.0	98.1
-Spot 63	231	122057	0.9	5.4415	0.5	12.6700	1.8	0.5000	1.7	0.96	2613.9	37.3	2655.4	17.1	2687.2	8.6	2687.2	8.6	97.3

Table 03NA15. U-Pb geochronologic analyses.

						Isotope Ratios					Apparent Ages (Ma)								
Analysis	U (ppm)	206Pb 204Pb	U/Th	206Pb* 207Pb*	± (%)	207Pb* 235U*	± (%)	206Pb* 238U	± (%)	Error corr.	206Pb* 238U*	± (Ma)	207Pb* 235U	± (Ma)	206Pb* 207Pb*	± (Ma)	Best Age (Ma)	± (Ma)	Conc (%)
-Spot 52	279	89707	1.8	11.4424	0.9	2.8469	3.1	0.2363	3.0	0.96	1367.2	36.8	1368.0	23.5	1369.2	17.8	1369.2	17.8	99.9
-Spot 15	417	257168	0.9	11.4281	0.8	2.8133	3.0	0.2332	2.9	0.96	1351.1	35.2	1359.1	22.5	1371.6	15.8	1371.6	15.8	98.5
-Spot 50	499	134459	1.1	11.2926	0.8	2.8351	2.6	0.2322	2.4	0.96	1346.0	29.7	1364.9	19.2	1394.5	14.5	1394.5	14.5	96.5
-Spot 63	363	649621	11.5	11.1657	0.7	2.9960	2.9	0.2426	2.8	0.97	1400.3	35.8	1406.6	22.3	1416.1	13.9	1416.1	13.9	98.9
-Spot 87	174	23113	3.1	11.1589	0.7	3.0560	3.1	0.2473	3.0	0.97	1424.7	38.4	1421.7	23.6	1417.3	13.4	1417.3	13.4	100.5
-Spot 110	425	145411	1.6	11.1451	0.9	2.9741	3.0	0.2404	2.8	0.96	1388.8	35.5	1401.0	22.6	1419.7	16.6	1419.7	16.6	97.8
-Spot 77	216	24808	1.9	11.1161	0.9	3.1266	2.5	0.2521	2.4	0.94	1449.2	30.7	1439.3	19.4	1424.7	16.3	1424.7	16.3	101.7
-Spot 100	298	2185478	2.3	11.0124	0.8	3.1094	2.8	0.2483	2.7	0.96	1429.9	34.6	1435.0	21.7	1442.5	16.0	1442.5	16.0	99.1
-Spot 70	191	77411	2.1	11.0076	0.8	3.0412	3.7	0.2428	3.6	0.98	1401.2	45.4	1418.0	28.2	1443.4	15.0	1443.4	15.0	97.1
-Spot 33	152	211278	1.3	10.9942	0.7	3.0703	3.0	0.2448	2.9	0.97	1411.7	36.4	1425.3	22.6	1445.7	13.1	1445.7	13.1	97.7
-Spot 2	343	135788	1.3	10.9353	0.9	3.0326	2.5	0.2405	2.4	0.94	1389.4	29.6	1415.9	19.3	1455.9	16.7	1455.9	16.7	95.4
-Spot 6	655	20311	2.3	10.7386	0.8	3.1041	1.9	0.2418	1.7	0.91	1395.8	21.4	1433.7	14.4	1490.4	14.7	1490.4	14.7	93.7
-Spot 40	107	27573	2.0	9.7546	1.1	4.2663	2.9	0.3018	2.7	0.93	1700.4	40.0	1686.9	23.7	1670.1	19.8	1670.1	19.8	101.8
-Spot 51	262	235688	2.8	9.7503	0.7	4.3070	2.6	0.3046	2.5	0.97	1713.9	37.8	1694.7	21.4	1671.0	12.6	1671.0	12.6	102.6
-Spot 53	324	73334	3.4	9.7397	0.7	4.2297	2.8	0.2988	2.7	0.97	1685.3	40.5	1679.8	23.1	1673.0	12.8	1673.0	12.8	100.7
-Spot 72	112	17236	1.8	9.7262	0.8	4.2953	3.3	0.3030	3.2	0.97	1706.1	47.7	1692.5	27.1	1675.5	15.2	1675.5	15.2	101.8
-Spot 89	208	35774	3.3	9.7149	0.7	4.2334	3.4	0.2983	3.3	0.98	1682.8	49.3	1680.5	27.9	1677.7	12.7	1677.7	12.7	100.3
-Spot 44	107	22184	0.8	9.7066	0.9	4.2949	4.3	0.3024	4.2	0.98	1703.0	63.2	1692.4	35.6	1679.3	16.9	1679.3	16.9	101.4
-Spot 78	261	189015	1.5	9.6991	0.7	4.2395	2.5	0.2982	2.4	0.96	1682.5	35.7	1681.7	20.6	1680.7	12.6	1680.7	12.6	100.1
-Spot 65	225	20547	1.6	9.6892	0.7	4.2763	2.4	0.3005	2.3	0.96	1693.8	33.9	1688.8	19.6	1682.6	12.6	1682.6	12.6	100.7
-Spot 71	192	130215	1.8	9.6752	1.0	4.2541	3.1	0.2985	2.9	0.95	1683.9	43.0	1684.5	25.1	1685.3	17.8	1685.3	17.8	99.9
-Spot 104	331	223385	3.2	9.6609	0.7	4.3550	2.8	0.3051	2.7	0.96	1716.8	40.9	1703.9	23.2	1688.0	13.7	1688.0	13.7	101.7
-Spot 96	284	1228905	2.6	9.6529	0.8	4.3425	2.3	0.3040	2.1	0.94	1711.2	31.9	1701.5	18.7	1689.5	14.6	1689.5	14.6	101.3
-Spot 54	432	203210	1.2	9.6488	0.8	4.1721	2.3	0.2920	2.2	0.95	1651.3	32.3	1668.6	19.2	1690.3	14.1	1690.3	14.1	97.7
-Spot 48	86	40599	2.4	9.6401	0.8	4.3885	3.7	0.3068	3.6	0.98	1725.1	54.6	1710.2	30.5	1691.9	14.1	1691.9	14.1	102.0
-Spot 94	275	168544	3.6	9.6367	0.8	4.3001	2.9	0.3005	2.8	0.96	1694.0	41.7	1693.4	23.9	1692.6	14.4	1692.6	14.4	100.1
-Spot 74	206	216448	2.5	9.6317	0.7	4.1753	2.8	0.2917	2.7	0.97	1649.9	39.4	1669.2	22.9	1693.6	13.2	1693.6	13.2	97.4
-Spot 20	341	1233185	1.5	9.6315	0.7	4.2347	2.7	0.2958	2.6	0.96	1670.5	38.3	1680.8	22.2	1693.6	13.3	1693.6	13.3	98.6
-Spot 28	148	54039	2.2	9.6290	0.9	4.3028	3.3	0.3005	3.2	0.97	1693.7	47.5	1693.9	27.2	1694.1	15.7	1694.1	15.7	100.0
-Spot 14	286	46245	2.7	9.6106	0.8	4.3756	2.9	0.3050	2.8	0.96	1716.0	42.1	1707.8	24.1	1697.6	15.2	1697.6	15.2	101.1
-Spot 81	342	457099	1.4	9.6069	0.6	4.1673	2.5	0.2904	2.5	0.97	1643.3	35.6	1667.6	20.7	1698.3	11.2	1698.3	11.2	96.8
-Spot 97	174	71780	1.7	9.6054	0.7	4.3057	2.9	0.3000	2.8	0.97	1691.1	41.2	1694.5	23.6	1698.6	13.4	1698.6	13.4	99.6
-Spot 98	361	118770	2.4	9.5968	0.6	4.0255	2.5	0.2802	2.4	0.97	1592.3	34.4	1639.4	20.5	1700.2	11.6	1700.2	11.6	93.7
-Spot 49	577	77051	3.9	9.5937	0.8	3.9157	2.3	0.2725	2.1	0.93	1553.3	29.6	1616.9	18.6	1700.8	15.4	1700.8	15.4	91.3
-Spot 80	243	47992	2.8	9.5925	0.9	4.3740	2.4	0.3043	2.3	0.93	1712.6	34.4	1707.4	20.2	1701.1	16.0	1701.1	16.0	100.7
-Spot 17	25	6273	2.3	9.5865	1.4	4.4749	5.7	0.3111	5.5	0.97	1746.3	84.0	1726.3	47.1	1702.2	25.9	1702.2	25.9	102.6
-Spot 101	523	130343	4.6	9.5834	0.8	4.1803	2.2	0.2906	2.0	0.93	1644.3	29.5	1670.2	17.8	1702.8	14.3	1702.8	14.3	96.6
-Spot 107	234	29696	2.5	9.5831	0.7	4.3595	2.3	0.3030	2.2	0.96	1706.2	33.6	1704.7	19.3	1702.9	12.0	1702.9	12.0	100.2
-Spot 35	268	464320	3.0	9.5759	0.8	4.2548	2.7	0.2955	2.6	0.96	1668.9	38.0	1684.7	22.1	1704.3	13.8	1704.3	13.8	97.9
-Spot 41	176	78373	2.0	9.5729	0.9	4.2911	2.9	0.2979	2.8	0.95	1681.0	41.2	1691.7	24.1	1704.8	16.4	1704.8	16.4	98.6
-Spot 10	231	73466	4.8	9.5718	0.7	4.3921	2.9	0.3049	2.8	0.97	1715.6	42.6	1710.8	24.2	1705.1	13.6	1705.1	13.6	100.6
-Spot 106	548	678532	3.2	9.5715	0.6	4.5405	2.3	0.3152	2.2	0.96	1766.2	33.6	1738.4	18.8	1705.1	11.2	1705.1	11.2	103.6
-Spot 75	470	217148	1.5	9.5690	0.7	4.3574	2.6	0.3024	2.5	0.96	1703.3	38.0	1704.3	21.8	1705.6	13.3	1705.6	13.3	99.9
-Spot 105	221	128229	2.4	9.5665	0.7	4.4519	2.5	0.3089	2.4	0.96	1735.2	36.8	1722.1	20.8	1706.1	12.8	1706.1	12.8	101.7
-Spot 82	176	38840	2.8	9.5658	0.9	4.3713	2.6	0.3033	2.4	0.94	1707.5	36.4	1706.9	21.3	1706.2	16.1	1706.2	16.1	100.1
-Spot 76	177	52429	2.6	9.5655	0.7	4.3983	2.3	0.3051	2.2	0.96	1716.7	33.5	1712.0	19.2	1706.3	12.3	1706.3	12.3	100.6
-Spot 109	354	108768	3.9	9.5630	0.9	4.4368	3.4	0.3077	3.3	0.97	1729.5	50.4	1719.2	28.5	1706.7	16.4	1706.7	16.4	101.3
-Spot 25	226	248995	1.9	9.5614	0.8	4.3719	3.1	0.3032	3.0	0.96	1707.0	45.5	1707.0	26.0	1707.1	15.2	1707.1	15.2	100.0
-Spot 19	270	40230	1.6	9.5573	0.7	4.1069	3.0	0.2847	2.9	0.97	1614.9	41.7	1655.7	24.5	1707.8	12.6	1707.8	12.6	94.6
-Spot 95	173	168062	2.2	9.5550	0.8	4.3718	2.8	0.3030	2.7	0.96	1706.0	40.2	1707.0	23.1	1708.3	14.2	1708.3	14.2	99.9
-Spot 8	172	25914	1.9	9.5540	0.9	4.3864	3.3	0.3039	3.2	0.96	1710.8	47.4	1709.8	27.1	1708.5	16.2	1708.5	16.2	100.1
-Spot 37	142	30495	1.7	9.5537	0.8	4.2360	3.2	0.2935	3.1	0.96	1659.1	45.2	1681.0	26.3	1708.5	15.6	1708.5	15.6	97.1
-Spot 83	426	81284	1.5	9.5497	0.7	3.8972	2.9	0.2699	2.8	0.97	1540.4	38.0	1613.1	23.1	1709.3	12.7	1709.3	12.7	90.1
-Spot 12	151	1556626	2.6	9.5488	0.8	4.3757	3.1	0.3030	3.0	0.96	1706.3	44.4	1707.8	25.4	1709.5	14.9	1709.5	14.9	99.8
-Spot 16	476	379213	3.0	9.5441	0.8	4.3462	2.4	0.3008	2.3	0.95	1695.5	33.8	1702.2	19.7	1710.4	14.0	1710.4	14.0	99.1
-Spot 45	157	185284	2.2	9.5417	0.7	4.3241	2.9	0.2992	2.8	0.97	1687.5	41.8	1698.0	23.9	1710.8	13.1	1710.8	13.1	98.6
-Spot 9	194	128261	3.1	9.5329	0.9	4.2746	3.1	0.2955	2.9	0.95	1669.2	43.2	1688.5	25.4	1712.5	17.2	1712.5	17.2	97.5
-Spot 36	151	30328	1.8	9.5218	0.8	4.3288	2.4	0.2989	2.3	0.95	1686.1	34.4	1698.9	20.1	1714.7	13.8	1714.7	13.8	98.3
-Spot 108	191	153463	1.7	9.5214	0.8	4.3236	3.0	0.2986	2.9	0.97	1684.2	42.3	1697.9	24.4	1714.8	13.9	1714.8	13.9	98.2

						Isotope Ratios					Apparent Ages (Ma)								
Analysis	U (ppm)	206Pb 204Pb	U/Th	206Pb* 207Pb*	± (%)	207Pb* 235U*	± (%)	206Pb* 238U	± (%)	Error corr.	206Pb* 238U*	± (Ma)	207Pb* 235U	± (Ma)	206Pb* 207Pb*	± (Ma)	Best Age (Ma)	± (Ma)	Conc (%)
-Spot 42	346	52312	1.8	9.5187	0.6	4.2700	2.8	0.2948	2.8	0.98	1665.4	40.5	1687.6	23.2	1715.3	10.6	1715.3	10.6	97.1
-Spot 56	476	259347	2.0	9.5181	0.7	4.3632	2.5	0.3012	2.3	0.96	1697.2	35.1	1705.4	20.3	1715.4	13.0	1715.4	13.0	98.9
-Spot 18	240	29281	1.2	9.5147	0.6	4.0993	2.5	0.2829	2.4	0.97	1605.9	34.2	1654.2	20.3	1716.1	11.1	1716.1	11.1	93.6
-Spot 30	284	87722	2.0	9.5121	0.9	4.3166	3.3	0.2978	3.1	0.96	1680.4	46.4	1696.5	26.9	1716.6	16.7	1716.6	16.7	97.9
-Spot 47	133	188460	3.0	9.5058	0.9	4.5363	3.4	0.3127	3.3	0.97	1754.2	50.6	1737.6	28.3	1717.8	15.8	1717.8	15.8	102.1
-Spot 13	528	656572	1.1	9.5056	0.7	4.4574	2.4	0.3073	2.3	0.95	1727.4	35.0	1723.1	20.1	1717.8	13.4	1717.8	13.4	100.6
-Spot 59	131	121855	1.9	9.5028	0.6	4.4731	2.2	0.3083	2.1	0.96	1732.3	32.7	1726.0	18.6	1718.4	11.3	1718.4	11.3	100.8
-Spot 67	655	37347	0.9	9.4986	0.7	3.7104	2.1	0.2556	2.0	0.94	1467.3	26.2	1573.6	17.0	1719.2	13.5	1719.2	13.5	85.4
-Spot 43	387	88370	2.1	9.4978	0.7	3.9355	2.6	0.2711	2.5	0.96	1546.4	34.7	1621.0	21.3	1719.3	13.7	1719.3	13.7	89.9
-Spot 91	119	68545	2.3	9.4978	0.6	4.3979	3.5	0.3029	3.5	0.99	1705.9	52.2	1711.9	29.2	1719.3	10.8	1719.3	10.8	99.2
Spot 103	309	1317308	3.0	9.4931	0.6	4.3578	2.6	0.3000	2.5	0.97	1691.5	37.0	1704.4	21.1	1720.2	10.5	1720.2	10.5	98.3
-Spot 57	290	38471	1.6	9.4923	0.8	4.3719	2.3	0.3010	2.1	0.93	1696.2	31.9	1707.0	18.9	1720.4	15.2	1720.4	15.2	98.6
-Spot 64	129	223956	2.2	9.4787	0.8	4.4075	3.1	0.3030	3.0	0.97	1706.2	45.3	1713.7	25.9	1723.0	14.5	1723.0	14.5	99.0
-Spot 11	297	36839	2.4	9.4745	0.6	4.0461	2.6	0.2780	2.5	0.97	1581.5	35.0	1643.5	20.9	1723.8	11.4	1723.8	11.4	91.7
-Spot 1	223	1623339	3.0	9.4637	0.7	4.6983	2.7	0.3225	2.5	0.96	1801.8	40.0	1766.9	22.2	1725.9	13.6	1725.9	13.6	104.4
-Spot 69	247	47778	6.6	9.4634	0.7	4.3618	3.0	0.2994	2.9	0.97	1688.2	43.1	1705.1	24.6	1726.0	12.5	1726.0	12.5	97.8
-Spot 5	276	606022	3.1	9.4592	0.8	4.4527	3.2	0.3055	3.1	0.97	1718.4	46.7	1722.2	26.4	1726.8	14.0	1726.8	14.0	99.5
-Spot 88	313	71594	2.3	9.4420	0.7	4.1597	2.8	0.2849	2.7	0.97	1615.8	38.1	1666.1	22.6	1730.2	13.1	1730.2	13.1	93.4
-Spot 93	338	236620	1.3	9.4385	0.9	4.4368	2.7	0.3037	2.5	0.94	1709.7	37.6	1719.2	22.1	1730.8	16.5	1730.8	16.5	98.8
-Spot 92	313	142398	1.3	9.4351	0.7	4.1497	2.4	0.2840	2.3	0.96	1611.3	33.3	1664.2	20.0	1731.5	13.0	1731.5	13.0	93.1
-Spot 27	64	18834	4.6	9.4322	1.0	4.4696	3.7	0.3058	3.5	0.97	1719.8	53.3	1725.3	30.4	1732.0	17.6	1732.0	17.6	99.3
-Spot 32	311	123223	2.0	9.4315	0.7	4.3889	2.8	0.3002	2.7	0.97	1692.4	40.4	1710.2	23.1	1732.2	12.3	1732.2	12.3	97.7
-Spot 3	218	225689	3.1	9.4066	0.9	4.6702	2.9	0.3186	2.7	0.95	1783.0	42.5	1761.9	24.0	1737.0	16.4	1737.0	16.4	102.6
-Spot 46	231	106963	1.5	9.3902	0.8	4.4607	2.7	0.3038	2.6	0.95	1710.1	38.5	1723.7	22.3	1740.2	14.8	1740.2	14.8	98.3
-Spot 29	104	24052	3.6	9.3669	0.9	4.4608	2.8	0.3030	2.7	0.95	1706.4	40.2	1723.7	23.4	1744.8	15.9	1744.8	15.9	97.8
-Spot 86	291	65231	8.6	9.3541	0.7	4.6307	3.0	0.3142	2.9	0.97	1761.1	44.3	1754.8	24.7	1747.3	12.9	1747.3	12.9	100.8
-Spot 26	210	55268	0.9	9.3505	0.8	4.5383	2.9	0.3078	2.8	0.97	1729.7	43.0	1738.0	24.5	1748.0	14.1	1748.0	14.1	99.0
-Spot 7	670	14505	2.3	9.3472	0.8	3.9346	2.3	0.2667	2.2	0.94	1524.2	29.3	1620.8	18.7	1748.6	14.8	1748.6	14.8	87.2
-Spot 39	162	139914	2.8	9.3265	0.8	4.5249	3.5	0.3061	3.4	0.97	1721.4	51.4	1735.6	29.2	1752.7	15.4	1752.7	15.4	98.2
-Spot 90	167	46041252	2.7	9.2161	0.9	4.6483	3.2	0.3107	3.1	0.96	1744.2	46.8	1758.0	26.7	1774.5	16.5	1774.5	16.5	98.3
-Spot 99	711	19802	4.2	9.1911	0.7	4.4375	2.5	0.2958	2.4	0.96	1670.5	35.7	1719.4	20.9	1779.4	12.2	1779.4	12.2	93.9
-Spot 79	218	39317	3.2	9.1572	0.8	4.6965	3.1	0.3119	3.0	0.96	1750.1	45.3	1766.6	25.7	1786.1	15.1	1786.1	15.1	98.0
-Spot 73	398	44745	2.2	9.0427	0.7	4.6953	2.7	0.3079	2.6	0.97	1730.6	39.6	1766.4	22.6	1809.0	12.2	1809.0	12.2	95.7
-Spot 84	506	138454	3.4	9.0138	0.8	4.6865	2.7	0.3064	2.5	0.96	1722.8	38.5	1764.8	22.3	1814.9	14.1	1814.9	14.1	94.9
-Spot 58	151	2283415	1.8	8.8865	0.8	4.9630	3.2	0.3199	3.1	0.97	1789.1	48.0	1813.0	26.7	1840.7	13.9	1840.7	13.9	97.2
-Spot 38	382	4284	2.2	8.7364	1.9	4.6917	3.3	0.2973	2.7	0.81	1677.8	40.1	1765.8	28.0	1871.5	35.2	1871.5	35.2	89.7
-Spot 22	344	26165	2.3	7.6409	0.9	5.8798	3.3	0.3258	3.2	0.97	1818.2	51.0	1958.3	28.9	2109.7	15.1	2109.7	15.1	86.2
-Spot 60	182	798900	1.8	7.4183	0.7	7.5504	2.4	0.4062	2.3	0.95	2197.7	42.3	2179.0	21.3	2161.4	12.4	2161.4	12.4	101.7
-Spot 24	268	64417	2.6	6.2246	0.9	9.9947	3.0	0.4512	2.9	0.95	2400.6	58.1	2434.3	28.1	2462.5	15.7	2462.5	15.7	97.5
-Spot 21	279	51930	0.6	6.0062	0.8	11.2041	2.9	0.4881	2.8	0.96	2562.3	58.3	2540.3	26.7	2522.7	12.6	2522.7	12.6	101.6
-Spot 62	413	1529666	1.5	5.9917	0.7	9.8118	2.4	0.4264	2.3	0.95	2289.4	44.8	2417.3	22.5	2526.7	12.2	2526.7	12.2	90.6
-Spot 4	504	3091544	1.1	5.7168	0.6	12.1821	2.3	0.5051	2.3	0.97	2635.7	48.7	2618.5	21.8	2605.3	9.9	2605.3	9.9	101.2
Spot 102	702	15551	1.4	5.5280	0.6	9.9607	2.4	0.3994	2.3	0.97	2166.1	43.0	2431.1	22.3	2661.1	9.9	2661.1	9.9	81.4
-Spot 66	118	64140	1.0	5.3908	0.7	13.2969	3.0	0.5199	2.9	0.97	2698.7	64.2	2701.0	28.4	2702.7	12.2	2702.7	12.2	99.9
-Spot 68	478	62289	1.2	4.7786	0.9	15.4828	2.9	0.5366	2.7	0.95	2769.2	61.4	2845.4	27.5	2899.9	15.0	2899.9	15.0	95.5
-Spot 31	96	4568064	3.5	4.6473	0.9	17.7382	3.5	0.5979	3.3	0.97	3021.3	80.7	2975.6	33.3	2944.9	14.1	2944.9	14.1	102.6

Table 05NA15. U-Pb geochronologic analyses.

						Isotope Ratios					Apparent Ages (Ma)								
Analysis	U (ppm)	206Pb 204Pb	U/Th	206Pb* 207Pb*	± (%)	207Pb* 235U*	± (%)	206Pb* 238U	± (%)	Error corr.	206Pb* 238U*	± (Ma)	207Pb* 235U	± (Ma)	206Pb* 207Pb*	± (Ma)	Best Age (Ma)	± (Ma)	Conc (%)
-Spot 12	183	36723	1.7	11.1089	0.6	2.9932	2.6	0.2412	2.5	0.97	1392.7	31.3	1405.9	19.6	1425.9	11.6	1425.9	11.6	97.7
-Spot 24	384	56951	1.7	11.0589	0.6	3.1372	2.1	0.2516	2.0	0.96	1446.8	26.4	1441.9	16.4	1434.5	11.8	1434.5	11.8	100.9
-Spot 69	136	22007	1.2	10.9740	0.6	3.1633	2.7	0.2518	2.6	0.98	1447.6	33.8	1448.3	20.6	1449.2	11.2	1449.2	11.2	99.9
-Spot 85	99	25802	2.8	10.9653	0.7	3.1243	2.6	0.2485	2.5	0.96	1430.6	31.9	1438.7	19.9	1450.7	13.7	1450.7	13.7	98.6
-Spot 105	173	62353	1.1	10.9274	0.6	3.0416	2.5	0.2411	2.4	0.97	1392.2	30.1	1418.1	18.9	1457.3	11.0	1457.3	11.0	95.5
-Spot 91	63	61174	2.6	10.8947	0.9	3.1980	3.4	0.2527	3.2	0.96	1452.4	42.1	1456.7	26.1	1463.0	17.7	1463.0	17.7	99.3
-Spot 71	392	24137	0.9	10.6836	0.6	3.2200	1.8	0.2495	1.7	0.94	1435.9	21.5	1462.0	13.7	1500.1	11.5	1500.1	11.5	95.7
-Spot 2	568	266996	4.6	9.7231	0.5	4.1744	1.9	0.2944	1.8	0.96	1663.3	26.9	1669.0	15.7	1676.1	10.0	1676.1	10.0	99.2
-Spot 79	65	10193	1.4	9.6272	0.8	4.3891	3.2	0.3065	3.1	0.97	1723.2	46.2	1710.3	26.1	1694.4	15.0	1694.4	15.0	101.7
-Spot 65	340	184834	3.5	9.6158	0.4	4.3668	1.4	0.3045	1.3	0.95	1713.8	19.8	1706.1	11.5	1696.6	8.1	1696.6	8.1	101.0
-Spot 46	123	14999	2.6	9.6103	0.8	4.3404	2.7	0.3025	2.6	0.96	1703.8	39.5	1701.1	22.6	1697.7	14.0	1697.7	14.0	100.4
-Spot 25	273	101518	1.9	9.5939	0.5	4.5485	2.1	0.3165	2.0	0.97	1772.6	31.6	1739.9	17.6	1700.8	9.9	1700.8	9.9	104.2
-Spot 102	110	17746	4.7	9.5754	0.6	4.3244	2.9	0.3003	2.9	0.98	1692.9	42.8	1698.0	24.3	1704.4	11.7	1704.4	11.7	99.3
-Spot 14	205	35491	2.0	9.5629	0.5	4.4277	2.8	0.3071	2.7	0.98	1726.4	40.9	1717.5	22.8	1706.8	9.9	1706.8	9.9	101.1
-Spot 59	242	52389	2.5	9.5517	0.6	4.3858	2.4	0.3038	2.3	0.96	1710.3	35.3	1709.7	20.2	1708.9	11.9	1708.9	11.9	100.1
-Spot 76	509	1639010	8.8	9.5228	0.5	4.4169	2.2	0.3051	2.1	0.98	1716.3	32.0	1715.5	18.0	1714.5	8.5	1714.5	8.5	100.1
-Spot 17	287	200636	3.3	9.5089	0.5	4.5622	2.3	0.3146	2.2	0.97	1763.5	34.3	1742.4	19.0	1717.2	9.6	1717.2	9.6	102.7
-Spot 49	271	101551	2.0	9.5074	0.5	4.4352	2.1	0.3058	2.1	0.98	1720.1	31.7	1718.9	17.8	1717.5	8.6	1717.5	8.6	100.2
-Spot 110	131	57214	2.4	9.5010	0.7	4.5626	3.0	0.3144	2.9	0.97	1762.3	44.9	1742.5	25.0	1718.7	13.6	1718.7	13.6	102.5
-Spot 35	322	323164	1.9	9.4960	0.7	4.4635	2.0	0.3074	1.9	0.94	1727.9	28.1	1724.2	16.4	1719.7	12.8	1719.7	12.8	100.5
-Spot 107	172	54278	3.9	9.4960	0.5	4.4300	1.9	0.3051	1.8	0.97	1716.6	27.4	1718.0	15.6	1719.7	8.8	1719.7	8.8	99.8
-Spot 4	627	2088593	2.3	9.4804	0.5	4.4869	1.9	0.3085	1.8	0.96	1733.4	27.9	1728.6	15.8	1722.7	9.5	1722.7	9.5	100.6
-Spot 30	299	128896	3.4	9.4733	0.6	4.5139	2.4	0.3101	2.4	0.97	1741.4	36.0	1733.5	20.2	1724.1	11.1	1724.1	11.1	101.0
-Spot 37	201	30891	1.5	9.4661	0.5	4.5470	2.1	0.3122	2.0	0.97	1751.4	30.9	1739.6	17.3	1725.5	9.4	1725.5	9.4	101.5
-Spot 43	659	231886	2.0	9.4609	0.5	4.4687	2.0	0.3066	1.9	0.96	1724.1	28.9	1725.2	16.5	1726.5	9.8	1726.5	9.8	99.9
-Spot 5	476	40692	1.4	9.4556	0.6	4.0614	2.1	0.2785	2.0	0.95	1583.9	28.3	1646.6	17.2	1727.5	11.5	1727.5	11.5	91.7
-Spot 44	143	488987	1.0	9.4512	0.7	4.4930	2.6	0.3080	2.5	0.96	1730.8	37.8	1729.7	21.4	1728.4	12.5	1728.4	12.5	100.1
-Spot 90	241	88175	1.3	9.4362	0.5	4.5846	2.5	0.3138	2.5	0.98	1759.2	38.3	1746.5	21.1	1731.3	8.9	1731.3	8.9	101.6
-Spot 99	101	157095	1.2	9.4145	0.7	4.5865	2.9	0.3132	2.8	0.97	1756.3	42.8	1746.8	24.0	1735.5	13.3	1735.5	13.3	101.2
-Spot 89	171	38730	1.0	9.3850	0.9	4.6579	3.2	0.3170	3.1	0.96	1775.3	48.0	1759.7	26.8	1741.3	15.8	1741.3	15.8	102.0
-Spot 92	122	60097	1.6	9.3691	0.7	4.5769	2.3	0.3110	2.2	0.95	1745.6	33.2	1745.1	19.1	1744.4	13.2	1744.4	13.2	100.1
-Spot 98	325	92773	1.1	9.3691	0.7	4.5582	2.0	0.3097	1.9	0.94	1739.4	29.3	1741.7	17.0	1744.4	12.4	1744.4	12.4	99.7
-Spot 61	100	140935	1.9	9.3560	0.7	4.5669	3.7	0.3099	3.7	0.98	1740.2	55.8	1743.2	31.1	1746.9	13.5	1746.9	13.5	99.6
-Spot 95	141	27364	1.1	9.3516	0.6	4.6730	2.9	0.3169	2.8	0.98	1774.8	43.4	1762.4	24.0	1747.8	11.3	1747.8	11.3	101.5
-Spot 18	102	25488	1.6	9.3477	0.6	4.6995	3.3	0.3186	3.3	0.98	1782.9	50.8	1767.2	27.8	1748.5	11.4	1748.5	11.4	102.0
-Spot 54	172	160732	3.3	9.3475	0.7	4.7174	2.7	0.3198	2.6	0.97	1788.8	41.0	1770.3	22.7	1748.6	12.4	1748.6	12.4	102.3
-Spot 88	300	99710	1.8	9.3418	0.4	4.6853	2.1	0.3174	2.0	0.98	1777.2	31.5	1764.6	17.3	1749.7	7.9	1749.7	7.9	101.6
-Spot 94	200	53595	2.4	9.3064	0.7	4.6430	2.4	0.3134	2.3	0.96	1757.4	35.9	1757.0	20.3	1756.7	12.1	1756.7	12.1	100.0
-Spot 47	215	1010027	1.9	9.2716	0.5	4.7067	2.1	0.3165	2.0	0.97	1772.6	31.5	1768.4	17.5	1763.5	8.6	1763.5	8.6	100.5
-Spot 101	177	36020	4.6	9.2477	0.6	4.6727	2.3	0.3134	2.2	0.97	1757.4	33.6	1762.4	18.9	1768.2	10.5	1768.2	10.5	99.4
-Spot 93	259	784972	3.4	9.2419	0.4	4.6907	2.4	0.3144	2.4	0.98	1762.4	36.5	1765.6	20.1	1769.4	7.8	1769.4	7.8	99.6
-Spot 84	424	143492	1.8	9.2417	0.6	4.7426	2.0	0.3179	1.9	0.95	1779.4	29.8	1774.8	16.9	1769.4	11.5	1769.4	11.5	100.6
-Spot 97	474	167560	1.4	9.2372	0.5	4.7505	1.7	0.3183	1.6	0.96	1781.2	25.3	1776.2	14.2	1770.3	8.6	1770.3	8.6	100.6
-Spot 31	212	50166	3.4	9.2368	0.6	4.8310	2.0	0.3236	1.9	0.95	1807.5	29.2	1790.3	16.5	1770.4	11.3	1770.4	11.3	102.1
-Spot 82	368	92024	3.1	9.2343	0.5	4.7653	1.7	0.3191	1.7	0.95	1785.6	25.8	1778.8	14.6	1770.9	9.8	1770.9	9.8	100.8
-Spot 62	119	107227	0.8	9.2297	0.7	4.5948	2.8	0.3076	2.7	0.97	1728.8	40.7	1748.3	23.1	1771.8	11.9	1771.8	11.9	97.6
-Spot 103	797	26724	3.2	9.2018	0.6	4.1472	2.0	0.2768	1.8	0.94	1575.1	25.8	1663.7	16.0	1777.3	11.7	1777.3	11.7	88.6
-Spot 48	200	48024	1.7	9.1988	0.7	4.7476	2.8	0.3167	2.8	0.97	1773.8	42.7	1775.7	23.8	1777.9	12.9	1777.9	12.9	99.8
-Spot 15	144	688978	3.8	9.1842	0.7	4.8367	3.1	0.3222	3.0	0.97	1800.3	47.9	1791.3	26.3	1780.8	12.9	1780.8	12.9	101.1
-Spot 10	133	220607	1.6	9.1802	0.7	4.7414	2.6	0.3157	2.5	0.97	1768.6	38.4	1774.6	21.5	1781.6	11.9	1781.6	11.9	99.3
-Spot 29	345	211645	3.6	9.1619	0.4	4.7614	2.1	0.3164	2.1	0.98	1772.1	32.5	1778.1	18.0	1785.2	7.6	1785.2	7.6	99.3
-Spot 19	121	42174	2.4	9.1605	0.7	4.8060	2.8	0.3193	2.7	0.97	1786.3	42.3	1785.9	23.6	1785.5	12.9	1785.5	12.9	100.0
-Spot 3	104	39221	5.6	9.1406	0.6	4.7993	3.2	0.3182	3.2	0.98	1780.7	49.7	1784.8	27.3	1789.5	10.6	1789.5	10.6	99.5
-Spot 73	229	64315	2.5	9.0657	0.6	5.0182	2.9	0.3299	2.8	0.97	1838.1	44.7	1822.4	24.3	1804.4	11.6	1804.4	11.6	101.9
-Spot 55	181	1659154	3.3	9.0648	0.7	4.9334	3.4	0.3243	3.3	0.98	1810.9	51.7	1808.0	28.3	1804.6	13.2	1804.6	13.2	100.3
-Spot 100	102	13794	2.5	9.0199	0.8	4.9754	3.4	0.3255	3.3	0.97	1816.5	52.1	1815.2	28.7	1813.6	14.5	1813.6	14.5	100.2
-Spot 42	263	1246184	4.2	9.0173	0.7	4.9043	2.2	0.3207	2.1	0.95	1793.3	32.5	1803.0	18.5	1814.2	12.7	1814.2	12.7	98.9
-Spot 26	157	64295	4.2	8.9961	0.7	5.1009	2.7	0.3328	2.6	0.96	1852.0	42.5	1836.3	23.3	1818.4	13.2	1818.4	13.2	101.8
-Spot 106	439	288686	2.2	8.9912	0.6	4.9813	1.8	0.3248	1.7	0.94	1813.3	26.2	1816.2	14.9	1819.4	11.0	1819.4	11.0	99.7
-Spot 20	239	104245	3.8	8.9692	0.6	4.9411	2.3	0.3214	2.3	0.97	1796.7	35.3	1809.3	19.6	1823.9	10.5	1823.9	10.5	98.5
-Spot 27	218	62499	1.7	8.9526	0.5	5.0560	2.5	0.3283	2.5	0.98	1830.1	39.5	1828.7	21.5	1827.2	9.1	1827.2	9.1	100.2
-Spot 96	140	61523	2.2	8.9294	0.6	5.1327	2.4	0.3324	2.3	0.97	1850.0	37.2	1841.5	20.2	1831.9	10.3	1831.9	10.3	101.0
-Spot 34	188	36449	1.9	8.9142	0.5	5.1249	2.3	0.3313	2.3	0.98	1844.9	36.4	1840.2	19.7	1835.0	9.1	1835.0	9.1	100.5

						Isotope Ratios					Apparent Ages (Ma)								
Analysis	U (ppm)	206Pb 204Pb	U/Th	206Pb* 207Pb*	± (%)	207Pb* 235U*	± (%)	206Pb* 238U	± (%)	Error corr.	206Pb* 238U*	± (Ma)	207Pb* 235U	± (Ma)	206Pb* 207Pb*	± (Ma)	Best Age (Ma)	± (Ma)	Conc (%)
-Spot 64	372	54845	2.5	8.8959	0.5	5.1977	1.8	0.3354	1.7	0.96	1864.3	27.7	1852.2	15.2	1838.7	9.1	1838.7	9.1	101.4
-Spot 67	208	134292	1.3	8.8814	0.8	5.2820	2.7	0.3402	2.6	0.95	1887.8	41.9	1866.0	23.0	1841.7	15.0	1841.7	15.0	102.5
-Spot 60	282	297676	2.3	8.8796	0.7	5.0304	3.3	0.3240	3.3	0.98	1809.0	51.6	1824.4	28.3	1842.1	11.8	1842.1	11.8	98.2
-Spot 87	203	1153897	4.4	8.8734	0.6	5.1301	2.3	0.3302	2.2	0.97	1839.1	35.0	1841.1	19.2	1843.3	10.5	1843.3	10.5	99.8
-Spot 57	400	38463	2.9	8.8066	0.7	4.7517	2.7	0.3035	2.6	0.97	1708.6	38.5	1776.4	22.3	1857.0	12.4	1857.0	12.4	92.0
-Spot 72	311	121869	1.9	8.7761	0.6	5.1797	2.3	0.3297	2.2	0.97	1836.9	35.2	1849.3	19.4	1863.3	10.5	1863.3	10.5	98.6
-Spot 21	190	17917	2.3	8.5689	0.9	5.5387	3.0	0.3442	2.9	0.95	1906.9	47.4	1906.6	26.0	1906.3	16.9	1906.3	16.9	100.0
-Spot 56	346	18935	1.2	8.5522	0.5	5.1878	2.4	0.3218	2.3	0.97	1798.4	36.3	1850.6	20.2	1909.8	9.8	1909.8	9.8	94.2
-Spot 109	378	3822721	1.7	8.5080	0.5	5.7119	2.1	0.3525	2.1	0.97	1946.3	34.7	1933.2	18.4	1919.1	9.7	1919.1	9.7	101.4
-Spot 36	585	378087	8.3	8.2965	1.6	5.4200	3.2	0.3261	2.8	0.86	1819.6	44.0	1888.0	27.6	1964.1	29.0	1964.1	29.0	92.6
-Spot 8	54	20421	0.6	8.1246	0.9	6.0304	4.7	0.3553	4.6	0.98	1960.0	77.5	1980.2	40.8	2001.4	16.3	2001.4	16.3	97.9
-Spot 70	552	119839	1.7	7.7781	0.6	6.6593	2.2	0.3757	2.1	0.96	2056.0	36.6	2067.2	19.1	2078.4	10.2	2078.4	10.2	98.9
-Spot 86	125	191086	1.2	6.9363	0.7	8.0477	2.5	0.4049	2.4	0.96	2191.4	44.3	2236.4	22.4	2277.9	11.5	2277.9	11.5	96.2
-Spot 39	179	55390	2.2	6.7009	0.5	8.7788	2.7	0.4266	2.6	0.98	2290.6	50.6	2315.3	24.3	2337.1	8.4	2337.1	8.4	98.0
-Spot 40	173	56190	0.5	6.3930	0.6	9.9237	2.6	0.4601	2.5	0.97	2440.1	50.4	2427.7	23.6	2417.3	10.2	2417.3	10.2	100.9
-Spot 13	625	203460	4.1	6.2684	0.5	9.9752	1.7	0.4535	1.6	0.96	2410.8	32.9	2432.5	15.7	2450.7	7.6	2450.7	7.6	98.4
-Spot 68	176	280756	2.3	6.2503	0.6	10.2221	2.7	0.4634	2.7	0.98	2454.5	54.7	2455.1	25.4	2455.6	9.9	2455.6	9.9	100.0
-Spot 81	318	158044	2.3	6.1969	0.6	10.3951	2.3	0.4672	2.2	0.96	2471.3	45.3	2470.6	21.2	2470.1	10.5	2470.1	10.5	100.0
-Spot 41	73	88716	1.7	6.1603	0.7	9.7548	3.5	0.4358	3.5	0.98	2331.9	68.0	2411.9	32.6	2480.1	11.3	2480.1	11.3	94.0
-Spot 66	179	306319	1.5	6.1500	0.5	10.6219	2.4	0.4738	2.4	0.98	2500.1	49.0	2490.6	22.5	2482.9	8.8	2482.9	8.8	100.7
-Spot 58	78	2207857	0.4	5.8181	0.8	11.2397	3.0	0.4743	2.9	0.97	2502.3	59.5	2543.2	27.7	2576.0	12.8	2576.0	12.8	97.1
-Spot 6	426	175413	0.9	5.6292	0.5	12.1665	2.1	0.4967	2.0	0.97	2599.7	42.7	2617.3	19.3	2631.0	8.6	2631.0	8.6	98.8
-Spot 1	566	25914	1.5	5.6240	0.6	11.5893	2.0	0.4727	1.9	0.96	2495.5	39.0	2571.8	18.4	2632.5	9.5	2632.5	9.5	94.8
-Spot 77	595	508323	1.6	5.5814	0.5	12.4031	1.9	0.5021	1.9	0.97	2622.7	40.6	2635.4	18.3	2645.2	7.8	2645.2	7.8	99.2
-Spot 83	383	102269	0.9	5.5391	0.5	11.9918	2.2	0.4817	2.1	0.97	2534.9	44.0	2603.8	20.3	2657.8	9.0	2657.8	9.0	95.4
-Spot 52	244	194612	0.9	5.5084	0.6	12.7486	2.4	0.5093	2.4	0.97	2653.7	51.4	2661.3	23.0	2667.0	10.0	2667.0	10.0	99.5
-Spot 78	250	154173	1.3	5.5009	0.6	12.8934	2.3	0.5144	2.2	0.97	2675.4	47.8	2671.9	21.2	2669.3	9.3	2669.3	9.3	100.2
-Spot 80	625	158200	1.4	5.4763	0.6	12.3770	2.0	0.4916	1.9	0.95	2577.5	41.2	2633.4	19.1	2676.7	10.3	2676.7	10.3	96.3
-Spot 11	91	715121	0.9	5.4422	0.5	13.6438	3.0	0.5385	3.0	0.98	2777.3	66.8	2725.3	28.4	2687.0	8.8	2687.0	8.8	103.4
-Spot 28	703	36502	3.5	5.4375	0.6	10.9133	2.1	0.4304	2.0	0.96	2307.4	39.2	2515.8	19.5	2688.4	9.2	2688.4	9.2	85.8
-Spot 32	350	280044	1.3	5.4343	0.7	13.1909	2.1	0.5199	2.0	0.94	2698.7	44.5	2693.4	20.2	2689.4	11.8	2689.4	11.8	100.3
-Spot 23	68	150492	1.5	5.3969	0.7	13.1049	4.5	0.5129	4.4	0.99	2669.2	96.6	2687.2	42.2	2700.8	11.5	2700.8	11.5	98.8
-Spot 51	178	34961	1.1	5.3883	0.6	13.5827	2.3	0.5308	2.2	0.97	2744.8	49.5	2721.1	21.7	2703.4	9.9	2703.4	9.9	101.5
-Spot 74	87	53893	1.5	5.3500	0.5	13.8203	2.6	0.5363	2.5	0.98	2767.8	57.3	2737.5	24.7	2715.2	9.0	2715.2	9.0	101.9
-Spot 45	82	91055	1.3	5.3341	0.8	13.2854	3.5	0.5140	3.4	0.97	2673.5	74.7	2700.1	33.2	2720.1	13.7	2720.1	13.7	98.3
-Spot 9	94	273739	1.1	5.3306	0.6	13.5592	2.9	0.5242	2.9	0.98	2717.0	63.3	2719.4	27.5	2721.2	9.4	2721.2	9.4	99.8
-Spot 53	353	142335	0.9	5.1574	0.5	14.2766	2.4	0.5340	2.3	0.97	2758.4	51.7	2768.3	22.5	2775.5	9.0	2775.5	9.0	99.4
-Spot 104	101	36439	1.2	3.3811	0.5	29.0384	3.4	0.7121	3.3	0.99	3466.3	89.2	3454.8	33.0	3448.2	7.1	3448.2	7.1	100.5

		Clear white Qtz, NE of Houlihan Springs Coyote Creek quad. Salmon quad has dip SW of 33 degrees.	
01NA15	Run	Same loc as Sherwin's sample that has Grenville aged zircons	N45 05' 21.38" W113 15' 31.56"
		Lonn stop #2 W of Rawhide Ck and E of W Coyote Creek. Salmon Map	
02NA15	Run	shows SE dip of 25 degrees	N15 04' 17.39" W113 16' 44.46"
		Feldspar poor qtz, Salmon Map shows as Cambrian Flathead?	
03NA15	Run	S of Brays Canyon along the road	N45 11' 40.58" W113 10' 13.37"
		Feldspathic Qtz with mud chips. Jahnke Lake Qtz?	
05NA15	Run	Left Fork of Buffalo Creek, Salmon Map shown as Yaj	N45 10' 22.25" W113 12' 25.10"